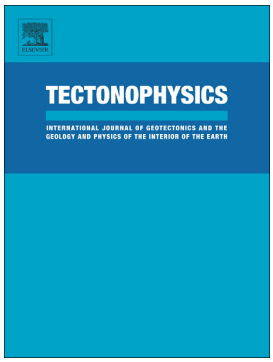

Upper mantle structure under the Zagros collision zone; insights from 3D teleseismic P-wave tomography

Mohammad Veisi, Farhad Sobouti, Sébastien Chevrot, Madjid Abbasi, Esmaeil Shabanian

PII: S0040-1951(21)00388-7

DOI: https://doi.org/10.1016/j.tecto.2021.229106

Reference: TECTO 229106

To appear in: *Tectonophysics*

Received date: 10 March 2021

Revised date: 10 September 2021

Accepted date: 5 October 2021

Please cite this article as: M. Veisi, F. Sobouti, S. Chevrot, et al., Upper mantle structure under the Zagros collision zone; insights from 3D teleseismic P-wave tomography, *Tectonophysics* (2021), https://doi.org/10.1016/j.tecto.2021.229106

Upper mantle structure under the Zagros Collision Zone; Insights from 3D teleseismic P-wave tomography

Mohammad Veisi[1], Farhad Sobouti[1], Sébastien Chevrot[2], Madjid Abbasi[3], Esmaeil Shabanian[1]

[1]*Department of Earth Sciences, Institute for Advanced Studies in Basic Sciences (IASBS), Zanjan Postal Code: 45137-66731, Iran.*

[2]*GET, UMR 5563, Observatoire Midi Pyrénées, Université Paul Sabatier, CNRS, IRD, Toulouse, France.*

[3]*Department of Surveying Engineering, University of Zanjan, Zanjan, Iran*

Abstract

We map the lateral variations of P-wave velocity beneath the Zagros collision zone in Iran down to 800 km depth by regional travel time tomography. We invert 32,293 relative travel time residuals from five temporary seismic networks across the collision zone in NW and central Zagros and northern Iran, and a large number of permanent stations distributed over the Iranian Plateau. A salient feature of our model is a ~225 km thick lithosphere beneath the Zagros, almost twice as thick as in the rest of Iran. Slab detachment at a depth range of 250-300 km from the base of the subducted continental Arabia is clearly distinguishable in central Zagros. In NW Zagros detachment appears to be at an earlier stage. Beneath the central Iran Plateau, we observe

shallow low-velocity regions down to 200 km depth, and smaller patches with significantly higher velocity in the 200-400 km depth range. This pattern could suggest a post-collisional foundering of the mantle lithosphere in the upper plate. The subducted slab seems to penetrate into the lower mantle in a segmented fashion, with no evidence for a stagnant slab above the 660 km interface.

Keywords: Traveltime tomography; Zagros Mountains; Iranian Plateau; Continental collision; Slab detachment; Lithospheric delamination

Introduction

The Iranian Plateau has formed as a result of the closure of the Neo-Tethys Ocean and the Arabia-Eurasia continental collision. Some of the more recent estimates put the onset of collision in the Oligocene (Egan et al., 2009; Agard et al., 2011; McQuarrie and van Hinsbergen, 2013; Pirouz et al., 2017). The Zagros Mountains on the southwestern margins of the plateau are the current locus of the collision in Iran (Fig. 1), accommodating a third of the total convergence of the Arabian platform under central Iran. The Main Zagros Thrust (MZT), the surface expression of the intracontinental suture (e.g., Stöcklin, 1968; Paul et al., 2006 and 2010), defines the northeast boundary of the Zagros range. Coeval with the deformation of the Zagros, mountain building processes and volcanism have been active in the Alborz Mountains in the north (e.g., Guest et al., 2006 and 2007; Ballato et al. 2010), while central Iran has experienced relatively recent plateau formation (5-10 Ma) and post-collisional volcanism (Omrani et al. 2008; Hatzfeld and Molnar, 2010; Chiu et al. 2013).

A thorough understanding of the Zagros collision zone and its Late Cenozoic history requires detailed tomographic images of upper mantle structures. Several questions, in particular, are

important in this regard; (1) What is the amount of lithospheric thickening since the onset of collision (2) Has this lithospheric thickening been limited to the margins of the upper plate, or did it propagate far into the plate interior in central Iran? (3) Has the collision resulted in an effective detachment of the oceanic slab from the underthrusting Arabian continental margin? (4) If the Iranian Plateau is the result of a late-stage lithospheric foundering/delamination, then, is there any evidence of that process left anywhere in the upper mantle?

Many body and surface wave tomographic studies from the global scale (e.g., Van der Meer et al., 2018) to the regional scale (e.g., Chang et al., 2010; Koulakov, 2011, Maggi and Priestley, 2005; Al-Lazki et al., 2004) have mapped the upper mantle seismic velocities and revealed the large-scale structure of the Tethyan subduction zone beneath the Zagros and Iranian Plateau. These studies have consistently found a high-velocity and thick lithosphere beneath the Zagros, whereas central Iran is characterized by a low velocity and thin lithosphere.

Local 2-D tomographic imaging of Iran was first performed by Kaviani et al. (2007) and many other studies have followed since (e.g., Paul et al., 2010; Motaghi et al., 2012; Rahmani et al., 2019; Mahmoodabadi et al., 2020). Several 3-D studies also focused on different regions of Iran (e.g., Shomali et al., 2011, Shad Manaman et al., 2011; Mahmoodabdi et al., 2019). These previous studies, which suffered from a rather limited station coverage, have confirmed the geometry of the underthrusted Arabian margin beneath central Iran and of the subducted oceanic slab. However, the available global tomographic models have poor resolution in the shallow upper mantle beneath Iran, mainly because of their coarse spatial discretization. On the other hand, regional-scale 2-D models, owing to their limited aperture (<600 km), have a poor resolution at depth, in particular in the mantle transition zone. In this study, we combine several datasets from permanent and temporary seismic networks installed in Iran to improve both the

aperture and ray coverage. The new extended dataset allows us to significantly improve the spatial resolution in both the shallow and deep parts of the mantle, providing key insights into the interaction of the two converging plates in the subduction zone and the fate of the subducted slab.

Data

Our dataset consists of teleseismic P-wave arrival times from 202 temporary, and 102 permanent stations in Iran (Fig. 1 and Table 1). The temporary stations belong to several arrays deployed at different times in various parts of the collision zone. The Zagros01 and Zagros03 arrays consist of two transects deployed in central and western Zagros for a few months in 2001 and 2003 respectively. The CIGSIP array operated for one year (2013-2014) along three parallel lines in western Iran covering the Zagros and Alborz mountains. The IASBS-CAM-1 (2008-2012) and IASBS-CAM-2 (2014-2016) arrays were installed in NW Iran and western Alborz, respectively, and operated for 6 to 30 months. We also use the data of the permanent stations of the Iranian national networks IRSC and INSN recorded between 2012 and 2019 to increase the resolution of our output model in the regions between the temporary arrays. With this distribution of seismic stations our tomographic study covers a significant part of the collision zone: NW and central Zagros, western and central Alborz, and a significant part of central Iran.

Data preparation and inversion method

We picked 32,293 first P-wave arrival times from 1588 teleseismic events with magnitudes greater than 5.5 and epicentral distances between 28^{o} and 95^{o} (Fig. 2a). For picking the relative P travel times we used the method developed by Chevrot (2002). The advantage of this method is that we can obtain robust and accurate travel time measurements even on very noisy data. The

travel times need to be corrected for crustal thickness, station elevation, and ellipticity of the Earth. For crustal thickness correction, we used the Moho depth map from Kaviani et al. (2020). We improved that map by including new crustal thicknesses estimated from P-wave receiver functions obtained from the temporary stations. We gridded the surface of the model with 15×15 km blocks. Inside each block, we determined the crustal thickness by interpolating from the nearest points available from the receiver functions and the Moho map. The station elevation corrections were calculated by computing the travel times between the surface of the WGS84 ellipsoid and the station elevations. We also corrected the travel times for the ellipticity of the Earth. We then computed average event travel times that were removed from the travel time residuals. These relative P-wave travel times were then inverted following the method of Aki et al. (1977), known as the ACH method.

Model parameterization in any inversion must follow some rules. The cell size in the uppermost layer of the model should not be smaller than the smallest distance between the stations, the depth to the bottom of the model should be no more than 2/3 of the largest station distances, and the cells should be large enough to contain sufficient ray crossings to prevent smearing in the output model (Evans and Achauer, 1993). We found that the choice of 25-km cubic cells was a good compromise and our model has been parameterized with 33 layers from the surface down to 825 km depth.

We added damping and smoothing constraints to regularize the inversion. The tomographic model is given by the solution of

$$J^T W_{obs} \delta \Delta t = (J^T W_{obs} J + W_{damp} + W_{smooth}) \Delta m, \qquad \text{Equation 1}$$

where $\delta\Delta t$ is the vector of relative traveltimes, J is the Jacobian matrix, W_{obs} is the weight matrix of the observations, W_{damp} is the damping matrix, W_{smooth} is the smoothing matrix and Δm is the vector of velocity perturbations. The Jacobian matrix for each event is given by

$$J_{ij} = (G_{ij} - \bar{G}_{ij}), \qquad \text{Equation 2}$$

where each element of G_{ij} is the travel time of the *i*th ray in the *j*th cell, and the elements of $\bar{G}_{ij}$are the averages of G_{ij} over all the stations that have recorded the event. Each element of the Jacobian is the travel time of the *i*th ray in the *j*th cell from which the mean travel time of all rays of the event passing through the cell is subtracted. The concept behind this modification is that $\bar{G}_{ij}\Delta m$ is equivalent to the mean travel time of each event, therefore, the modified Jacobian matrix has the effect of removing the average ray contribution. This eliminates the necessity for arbitrarily choosing one mean velocity as a reference. Recently, Maupin (2020) has shown that using demeaned event sensitivity kernels also removes the long wavelength biases arising from asynchronous station deployments. Therefore, our inversion scheme is well adapted to the joint inversion of travel time data coming from different permanent and temporary sub-arrays that may not have recorded the same number of events.

We regularize the inversion by adding damping and smoothing constraints. To smooth the solution, we damp the norm of the Laplacian of the model. The procedure for finding the optimum damping and smoothing coefficients is as follows. 1) We start the tomography with two initial damping and smoothing factors. 2) We run the inversion code iteratively inside two loops. The outer loop consists of 10 iterations over the damping factor, and the inner loop consists of 20 iterations over the smoothing factor. In this step 10 L-curves, one for each damping factor are

produced (see Figure S1 for selected L-curve). 3) We repeat steps 1 and 2 four times with different initial factors and increments to ensure that the best initial values are found. We pick the best L-curve from a set of 40. To choose the best damping and smoothing factors, we impose a RMS reduction of at least 50 percent, and a smooth final model not dominated by small-scale anomalies. The inversion achieved a final RMS reduction of 56.8%. The LSQR (Least Squares using the QR factorization) method of Paige and Saunders (1982) was used to solve the equations. This method is very fast and employs sparse matrix techniques.

We performed a synthetic checkerboard test to identify the parts of the model that are well resolved and to determine the amount of vertical smearing in regions of low ray density. In this test, the same complete ray distribution as in our real dataset has been used. The starting synthetic velocity model is made of 75-km cubic velocity anomalies organized in 3 horizontal layers in the shallow part of the model (< 450 km) and 2 layers of 100-km cubic anomalies in the deeper parts. The input velocity anomalies had ±5% perturbations. The synthetic blocks were placed at 50-125 km, 200-275 km, 350-425 km, 500-600 km, and 675-775 km depth. We also added 10% random noise to the synthetic relative residuals. The synthetic test achieved an RMS reduction of 62%. Fig. 3 shows the results of the test in layers 4, 10, 16, 23, and 30 of the model. In the shallow parts of the model (i.e., layer 4) the velocity variations are best resolved in regions of good station coverage. In the mid-upper mantle depths (i.e., layers 10 and 16) where ray crossing reaches its maximum, good resolving power is achieved in many parts of the model. In the deeper parts (i.e., layers 23 and 30), the ray density is distributed more evenly among the cells, and thus the inversion returns a more uniform pattern of velocity anomalies. Fig. 4 shows the results of the synthetic test along 7 cross-sections from northwest to southeast. In general, the resolution is good in the upper 400 km. In the regions far from the temporary arrays (e.g.,

sections d, e, and f) the near-surface anomalies show somewhat lower amplitudes with respect to the deeper features. Beneath the CIGSIP array and neighboring regions (section b), the resolution is good from the top to the bottom of the model. However, vertical smearing in the lower half of the model becomes significant in the northwestern part of the model (sections a, b and c).

Tomographic Results

Fig. 2b shows the average station residuals. Stations in the Zagros Mountains and the Sanandaj-Sirjan Zone (SSZ) are characterized by negative residuals. The most pronounced negative residuals are observed in NW Zagros. Positive residuals are observed in central Iran (including the UDMA), the Alborz Mountains, and NW Iran. Along the margins of the South Caspian Basin, the residuals are mostly negative.

Fig. 5 shows 12 horizontal plots of the velocity anomalies between 25 and 825 km depth. At shallow depths, the resolving power of the inversion is limited owing to the sub-vertical incidence of teleseismic P waves. The 25-50 km depth (Fig. 5a) corresponds to the lower crust throughout most of Iran. At this depth, the NW and central Zagros, and to some extent the SSZ, are characterized by high velocities, but in the middle part of the model, the high-velocities are limited to the Zagros and do not extend into the SSZ. Central Iran and the Alborz (with the exception of Caspian coastal areas) are characterized by low velocities in the lower crust. In the depth range corresponding to the lower lithosphere (75-175 km) the Zagros and the SSZ are again dominated by high-velocity anomalies, whereas in central Iran and central Alborz low velocities are observed. This suggests a strong and thick mantle root beneath the Zagros and a thinner lithosphere beneath central Iran. Between 200 and 325 km depth, the Zagros high-velocity anomalies gradually shift northeast across the boundary with central Iran, suggesting the

presence of a north-dipping lithospheric structure beneath the suture zone. In central Iran, a broad zone of high velocity appears between NW Zagros and Alborz. In the 375-825 km depth range, the most pronounced feature of the model is a broad high-velocity anomaly located beneath the SSZ and central Iran, whereas low velocities are observed beneath the Zagros.

Figures 6 and 7 show vertical sections across the tomographic model along 8 profiles. These profiles are ordered from northwest to southeast, with the distance axis origin set at the MZT. The velocity perturbations in most of the profiles are characterized by 4 major anomalous zones. The first anomaly, marked as ALH (Arabian Lithosphere High) is a shallow high-velocity feature beneath the Zagros and SSZ extending down to a depth of about 270-300 km. It also extends beneath central Iran by as much as 75 km north of the MZT (see also Fig. 5d). In the eastern half of the model, the anomaly is poorly resolved at shallower depth where station coverage is sparse (e.g., Fig. 7b and c). We interpret the ALH anomaly as the Arabian margin underthrusted beneath central Iran. The second anomaly marked as TSH (Tethyan Slab High), is a high-velocity region located north of the MZT under SSZ and central Iran. In most of the cross sections it is located below 400 km depth and extends to the bottom of the upper mantle, but in NW, as well as SE (Fig. 6k and l) it penetrates into the lower mantle as well. The resolution test (e.g., Fig. 4b-e) indicates that these features in the upper mantle are well resolved. We interpret the high-velocity TSH as the subducted Neotethyan slab. The third anomaly, marked as CIH (Central Iran High), is a high-velocity body beneath central Iran, observed at 200 km depth in the western part of the model. Towards the eastern regions and beneath central and eastern Alborz it gradually deepens to about 450 km depth (Fig. 7c). In the northern end of the profiles crossing the Alborz (e.g., Fig. 6a and b), a high-velocity shallow zone characterizes the transition between the Alborz Mountains and the South Caspian Basin, which suggests that the nature of the

Caspian lithosphere is different from the continental regions surrounding it. The fourth major anomalous zone in the model is the shallow low-velocity anomaly CIL (Central Iran Low) beneath central Iran and the Alborz. This anomaly is confined to the upper 150-200 km and reveals a thinner central Iran lithosphere bounded by the thick Zagros and South Caspian lithospheres.

Discussion

Seismic velocities in the Earth are influenced by temperature, anelasticity, partial melting, water content, and rock composition. Although the effect of anelasticity and rock composition can be largely ignored in the upper mantle where the oceanic slab is descending (Goes et al., 2000), isolating their relative contribution to the velocity field is challenging. In the following, we therefore assume that velocity perturbations mainly result from temperature anomalies.

Several scenarios have been proposed to explain the geodynamic evolution of the Arabia-Eurasia plate system. Among them, models suggested by Dercourt et al. (1993) and Şengör and Natal'in (1996) and another one by Stampfli and Borel (2002, 2004) have found wider acceptance. In the first model, except for a short-lived intra-oceanic subduction near the southern margin of the Neo-Tethys that resulted in the emplacement of the Oman ophiolites on the Arabian margin, all of the subduction has taken place at the northern margin of Neo-Tethys beneath Anatolia and central Iran. In the model proposed by Stampfli and Borel (2004) the subduction of the Neo-Tethys ridge beneath the Iranian blocks (Lut and SSZ) in the Mesozoic was followed by the opening of an intra-oceanic back-arc basin east of Arabia (the so-called Semail Ocean). During the Cenozoic, the Semail Ocean subducted beneath Eurasia. Hafkenscheid et al. (2006) used the above models to predict the present positions of Neo-Tethyan lithospheric domains subducted

since the Mesozoic. They compared their predictions with results from global mantle P-wave tomographies and concluded that most of the subducted Neo-Tethyan lithosphere is presently residing in the lower mantle between 800 and 2000 km depth. They further argued for the occurrence of an Early Oligocene slab detachment under the northern Zagros suture zone. According to this reconstruction, the high-velocity bodies presently observed in the mantle transition zone are mainly the Arabian margin lithosphere that has been pushed down since the Oligocene break-off and during the course of continental collision. Agard et al. (2011) presented a synthesis of various geological data to reconstruct the deformation history in the Zagros collision zone from 150 Ma to present. Their reconstruction is broadly similar to that of Hafkenscheid et al. (2006). They outlined a major slab break-off episode in Late Paleocene, and a more recent partial slab tear during the Miocene (~10 Ma) based on adakite formation in parts of the UDMA in central Iran (Omrani et al., 2008).

The structure of the Zagros lithosphere

Our model shows high velocities in the Zagros lithosphere and low velocities north of MZT in central Iran. A similar structure has been mapped in previous studies (e.g., Asudeh, 1982; Bijwaard et al., 1998; Kaviani et al., 2007; Shomali et al., 2011; Koulakov, 2011; Priestley et al., 2012; Mahmoodabadi et al., 2019). We interpret these anomalies as evidence for a colder and thicker lithosphere beneath the Zagros versus a thinner and warmer lithosphere in the surrounding regions. Priestley et al. (2012) used temperature modeling to derive the depth of the lithosphere-asthenosphere boundary from shear wave velocity profiles. They obtained a value of ~120 km for the thickness of the lithosphere everywhere except in the Zagros, for which their estimate was twice as much. Priestley et al. (2012) argued that the thickening of the Zagros lithosphere results from shortening. Motaghi et al. (2017a,b) inverted receiver functions from

seismic profiles in western and southern Zagros to derive shear wave velocity profiles, from which they inferred a deep LAB and thick lithosphere beneath the Zagros and SSZ (> 200 km). They interpreted this thickening as resulting from the underthrusting of the Arabian lithosphere beneath central Iran. Mohammadi et al. (2013) used P-to-S and S-to-P converted phases to constrain LAB depths of 130 and 150 km beneath western Zagros and SSZ, respectively, and significantly shallower depths of 80-90 km in central Iran and the Alborz. They also mapped a sharp lithospheric thickness variation between the SSZ and UDMA in central Iran. The P-wave tomography study by Mahmoodabadi et al. (2019) in western Zagros (coinciding with the region of Zagros03 array) also found a thick high-velocity lithospheric mantle beneath the Zagros and low-velocities beneath central Iran and Alborz.

The 2-D P-wave tomography of Rahmani et al. (2019) along the CIGSIP profile in NW Zagros showed a low-velocity wedge at a depth of 150 km near the frontal edge of the Arabian plate beneath the suture zone. They interpreted it as the beginning of the detachment of the lower part of the Arabian lithosphere from its upper part. The profile of Rahmani et al. (2019) coincides with our cross-section in Fig. 6c. We also identify a very thick lithosphere in the Zagros (anomaly ALH), but our model does not support a detachment of the Arabian lithosphere. Mahmoodabadi et al. (2020) also resolved a shallow low-velocity feature in NW Zagros south of the SSZ, and explained it as a narrow low-velocity corridor formed as a consequence of delamination of the Arabian lithosphere. In general, we observe a thick lithosphere along the strike of the Zagros throughout the range (e.g., Fig. 5b, c). However, important variations in the geometry of the frontal edge of the advancing Arabian plate are observed from NW to SE. In NW Zagros, the Arabian lithosphere achieves a maximum of 120 km of underthrusting beneath the SSZ at the location of the Zagros03 seismic line (Fig. 5d). In contrast, in central Zagros

(southeast of Zagros03 line in Fig 5) our model resolves low-amplitude velocity anomalies on both sides of the suture zone, with no clear evidence for significant underthrusting beneath central Iran. In SE Zagros, Motaghi et al. (2017b) observed evidence for lithospheric buckling with no indication of significant underthrusting of the Arabian lithosphere beneath central Iran. They argued that the abnormal thickness of the lithosphere could be the result of internal deformation of the Arabian lithosphere as it collides against the relatively strong central Iran lithosphere. Several previous tomographic studies have reported a similar non-cylindrical structure of the Zagros lithosphere along the collision zone. The P and S-wave imaging of the upper mantle in Iran by Alinaghi et al. (2007) and Koulakov (2011) show that central Zagros is underlain by a low velocity anomaly in the shallow upper mantle that is not observed beneath NW and SE Zagros, in good agreement with Chang et al. (2010) and Priestley et al. (2012).

The structure of the subducted slab

A prominent feature of our tomographic model is the combined ALH + TSH high-velocity region beneath the collision zone that extends from the surface down to the transition zone. In the southeastern part of the study region, it penetrates the lower mantle. The apparent dip of the structure is about 60°-70° towards northeast throughout the collision front. We interpret this structure as the underthrusting Arabian margin, still partially connected to the last fragments of the subducted oceanic slab, with a detachment around 200-300 km depth. The degree of detachment varies along the collision zone; whereas slab detachment seems to have remained at an early stage beneath NW Zagros, it seems more mature beneath central Zagros. The depth of detachment is just beneath the thickened Arabian lithosphere, and since the top of the detached slab is still observed at a shallow level, it might be a relatively recent event developed in the latter stages of collision. Omrani et al. (2008) documented a post-Late Miocene formation of

volcanic rocks with adakitic signature in UDMA in central Iran, and based on their spatially limited distribution along the arc, they inferred that they must have formed as a result of slab melting during a slab break-off event. Agard et al. (2011) expanded on this idea and used other geological evidence to suggest that a late partial break-off/tear caused the detachment of the Neo-Tethyan slab from the continental lithosphere at around 10 Ma. They also argued that the extent of break-off must be greater in central Zagros than in the northwest. A number of previous tomographic studies have provided evidence for slab detachment in the Zagros. Van der Meer et al. (2018) showed a tomographic image beneath northern Zagros where a detached slab segment with its top just below the Zagros root descends into the lower mantle. In western Zagros, Mahmoodabadi et al. (2019) evidenced a high-velocity anomaly at 300 km depth disconnected from the Zagros lithosphere. They interpreted it as a remnant of the Neo-Tethyan oceanic slab detached from the leading continental edge. Rahmani et al. (2019) in their tomography study on the CIGSIP array obtained a similar image. They found a pronounced high-velocity anomaly at depths greater than 350 km north of the Zagros suture and interpreted it as a remnant of the Neo-Tethyan slab. However, their tomographic model does not show a separation between the continental lithosphere at the surface and the remnant slab at depth. They performed a synthetic modeling and showed that the apparent continuity between the two high-velocity regions could be the result of smearing. Nevertheless, they stopped short of explicitly arguing for a slab detachment event.

The available evidence from seismic anisotropy is in good agreement with a slab detachment event beneath the Zagros, as well as to the generally-complex lithospheric thickness variations between the Zagros and central Iran as discussed in the previous section. Recent shear wave splitting studies by Sadeghi-Bagherabadi et al. (2018), Kaviani et al. (2021) and Arvin et al.

(2021) have revealed a complex mantle flow pattern beneath Iran compared to a simpler flow regime beneath the Anatolian Plateau and Arabian Plate, where lithospheric thickness varies relatively smoothly. Kaviani et al. (2021) hypothesized that the southwest mantle flow field is deflected beneath the Zagros by the lithospheric keel, producing a NW-SE toroidal flow beneath central Iran parallel to the strike of the collision zone. Similarly, Sadeghi-Bagherabadi et al. (2018) invoked a combination of the Zagros keel effect and an asthenospheric edge-driven convective flow beneath central Iran to explain the NW-SE fast splitting directions under the southwestern margin of central Iran. In NW Iran and the Alborz region where the lithosphere is thinner, the anisotropic fast-axis directions suggest a simple mantle flow field away from the collision zone. The inferred circular pattern around the Zagros keel implies sharp boundaries for the Zagros lithosphere, in good agreement with our tomography results. It also implies a gap in the slab to explain the mantle flow transfer to central Iran. This gap may have result from the slab detachment event. The proposed keel deflection and associated circular flow is mainly concentrated in NW and South central Zagros, coinciding with locations where we have evidenced slab detachments (i.e. profiles CR6 to CR12, and CR37 and region to its SE in Fig.6 and 7). The evidence from seismic anisotropy corroborates our evidence for slab detachment and furthermore, it indicates that the zone of detachment possibly has a significant role in the organization of the mantle flow field beneath the collision zone.

Most cross sections in NW Zagros image a Tethyan slab descending into the lower mantle directly. This feature is not as clear in the southern part of the model (e.g. profile CR37 in Fig.7). Kaviani et al. (2018) studied the variations of the mantle transition zone thickness beneath the Middle East. They identified a significant depression of the 660 boundary and a modest uplift of the 410 in NW Zagros, corresponding to our western profiles. They interpreted this feature as

resulting from the presence of a slab segment in western Zagros. In south central Zagros they observed the uplift of both 410 and 660 discontinuities, which precludes the presence of stagnant slab in that part of the mantle.

To evaluate the reliability of our tomographic model and assess the amount of smearing that may mask the distances between the prominent anomalous regions, we performed additional synthetic resolution experiments to test if the major anomalies observed in our tomographic model are adequately resolved. Specifically, we modelled the ALH, TSH, and CIH anomalies in the region encompassing the CIGSIP and Zagros03 arrays where there is good station coverage and ray-crossing density. Fig. 8 shows the results of the synthetic test. The real-data anomalies were modelled by uniform horizontal prisms placed across the western part of the model. The ALH anomaly had a polygonal shape with its base at 200 km depth. The TSH and CIH had rectangular sections. We varied the position of the top of the TSH prism, from 25 km to 175 km below the base of ALH. Fig. 8 illustrates the extent of vertical smearing in our inversions. In the 200-400 depth range, where ray crossing is maximum, horizontal boundaries have been displaced by as much as 50 km along the vertical direction. Vertical boundaries are much better resolved. In one model run we assumed an unbroken slab down to 650 km depth (Fig. 8d). The inversion returned a continuous unbroken high-velocity region from surface to bottom, a very different pattern from what is observed in the real-data tomography. Anomalous bodies vertically separated by more than 100 km can be resolved. We also observe that the geometry of the resolved synthetic anomalies changes by only a moderate amount between the various cross-sections. Overall, the structures beneath profiles CR 9 to 14 are the best resolved.

van Hunen and Allen (2011) quantitatively investigated slab break-off subsequent to continental subduction. They found that the mechanical strength of the slab has a major role in the timing of

slab break-off after the onset of collision. For an old and strong subducting slab this time is 20-25 Ma, while for a young and weak slab it can be as early as 10 Ma. van Hunen and Allen (2011) applied their findings to the Arabia-Eurasia collision zone by assuming an age of 35 Ma for the initial collision and a Permian age of 200 Ma for the subducting Neo-Tethyan slab. They deduced that slab break-off could not have occurred before 15-10 Ma. Better estimates now put the onset of collision in the Zagros at around 27-25 Ma (Egan et al., 2009; Agard et al., 2011 and references therein). Following van Hunen and Allen (2011), slab detachment in the Zagros could have occurred as recently as 5 Ma ago, significantly more recently than what the geological evidence suggests. This discrepancy can be resolved by assuming that the subducting slab was weaker than what is expected for its age. One can also argue that the actual slab break-off in the Zagros has been a faster process. In fact, numerical modeling by Duretz et al. (2011, 2012) incorporating a combination of viscous and Peierls creep mechanisms predicted that an 80 Ma old oceanic lithosphere subducting at a rate of 5 cm/yr can break off significantly sooner, at about 11 Ma after the onset of collision and at a depth of about 300 km. In terms of time and depth of break-off, the predictions by Duretz et al. (2011, 2012) are in good agreement with the available geological evidence and our tomography results in the Zagros. Since our tomographic images evidence a break off developed unevenly along the collision zone, this would suggest that the process is still ongoing.

The upper mantle structure beneath central Iran and the Alborz

In our model we observe slow velocities in the shallow upper mantle (<175 km) beneath central Iran and the Alborz (anomaly CIL). Voluminous high-velocity bodies are observed between 200 to 350 km depth (anomaly CIH), beneath the southern flank of the Alborz Mountains and adjacent regions in central Iran (e.g., Fig. 5e).

Previous studies have reported slow propagation of body and surface waves and high attenuation rates across the Turkish-Iranian Plateau (e.g., Al-Lazki et al., 2004; Maggi and Priestley, 2005; Al-Damegh et al., 2004; Kaviani et al., 2007; Mahmoodabadi et al., 2019). These observations have led many authors to suggest that central Iran has a thin lithosphere and a warm upper mantle. The LAB depth beneath the southern side of the Alborz Mountains calculated by Rastgoo et al. (2018) from receiver functions and dispersion curves is around 150 km. Central Iran is an elevated plateau with a surface relief of 1000-1500 m built during the course of the collision. Despite its relatively high topography, it is only moderately thickened compared to the Zagros. The measured Moho depths from receiver functions in central Iran range from 42 km north of the Zagros suture (Paul et al., 2006) to 48 km just south of the Alborz Mountains (Radjaee et al., 2010). Hatzfeld and Molnar (2010) through a detailed analysis of available geologic, present-day kinematics of deformation, and deep structure data, discussed the possibility of convective removal of the mantle lid in Tibet and in central Iran. They argued that the low seismic velocities in the uppermost mantle just below the Moho depth beneath both plateaus are consistent with Late-Cenozoic removal of the mantle lithosphere. Several recent seismic tomographies in Tibet have produced strong evidence for lithospheric foundering/delamination as a result of continental collision (Ren and Shen, 2008; Chen et al., 2017; Huang et al., 2019). The seismic structure of these models consists of a shallow low-velocity zone in the uppermost mantle sitting over a deeper high-velocity body that extends as deep as the mantle transition zone. In the central Iranian Plateau, the seismic structure of the upper mantle is much less clear than in Tibet and Hatzfeld and Molnar (2010) were not able to present unequivocal evidence from seismic tomography for convective removal of the mantle lithosphere. Seismological studies remain so far inconclusive on the hypothesis of mantle

delamination in central Iran. The low-resolution surface wave study by Maggi and Priestley (2005) in western Asia mapped a low-velocity upper mantle beneath central Iran which was interpreted as an indicator of a thin delaminated lithosphere and a warm shallow mantle. The regional P wave tomography by Mahmoodabadi et al. (2019) has revealed a similar low-velocity shallow structure, but the authors invoked the subduction model by Verdel et al. (2011) to explain their observations. According to Verdel et al. (2011), flat subduction beneath the Eurasian margin in the Cretaceous was followed by slab roll-back, extension, and magmatism in central Iran and asthenospheric upwelling during the Eocene, resulting in a pre-collisional thin lithosphere and warm upper mantle on the Eurasian side. Petrological evidence for post-collisional delamination in northern Iran comes from the region of Damavand, a Quaternary volcano in central Alborz. Davidson et al. (2004) and Liotard et al. (2008) argued that the geochemistry of the Damavand magmatism points to lithospheric delamination in the Alborz. Shabanian et al. (2012) analyzed structural controls on the Alborz volcanism in a post-collisional setting and proposed that the volcanic activity of Damavand has been the result of magma generation due to a rising asthenosphere following lithospheric delamination in a transtensional environment. Rastgoo et al. (2018) used their 2-D seismic profile along the southern flank of the Alborz Mountains to verify the structural model proposed by Shabanian et al. (2012). In western and central Alborz their model revealed a low-velocity layer in the 50-100 km depth range and a higher-velocity zone at 100-150 km depth. The spatial distribution of these velocity zones was interpreted as the result of post-collisional delamination of the lower part of the western Alborz lithosphere.

The previous seismological studies proposing delamination in central Iran, have only provided evidence for a thin “delaminated” lithosphere, without revealing anything that can be taken as

proof for the presence of the sunken root itself. In several of our profiles and depth plots, the high-velocity anomaly CIH can be spotted at different depths between 200 and 350 km. It is the best observed in the northern margin of central Iran and the southern side of the Alborz range. The CIH anomaly progressively deepens from northwest to southeast (compare successive profiles in Fig. 6 and 7), suggesting a foundering body at different stages of descent. We suggest that the CIH body might offer tangible evidence for the sunken root. In terms of depth interval and vertical configuration, the CIH anomaly is similar to what seismic studies mentioned above have described in Tibet. François et al. (2014) through numerical modeling of continental subduction, attempted to test the mechanisms for the buildup of dynamic topography in the central Iranian Plateau. They showed that a recent slab break-off (5-10 Ma) after the onset of collision, could have indirectly initiated a mantle flow field beneath the overriding plate, resulting in the delamination of the upper plate lithospheric mantle. A late-stage isostatic readjustment of the uplifted plateau would follow without undergoing significant crustal thickening. Their successful models were able to produce small-scale convective instabilities beneath the upper plate with wavelengths comparable to the size of the fast anomalies we have observed in our tomographic model.

Conclusions

Figure 9 summarizes our findings of the lithospheric and upper mantle structure beneath the Zagros collision zone. Our tomographic study documents variations of lithospheric thickness between the Zagros and central Iran and a post-collisional slab detachment around 250 km depth. If we assume that the detachment occurred right beneath the base of the subducted Arabian continental margin, then the maximum thickness of the continental root must be no greater than 225-250 km. This would imply a doubling of the Zagros lithosphere as a result of collision. The

absence of high-velocity anomalies far north of the MZT at the lithospheric depth range indicates that the lithosphere's thickening has not propagated into the interior of central Iran.

The high-velocity anomalies at 200-300 km depth beneath central Iran suggest the presence of fragments of delaminated mantle lithosphere. They also suggest a post-collisional slab break-off in central Zagros which seems to be at an earlier stage in NW Zagros compared to central Zagros. From the shallow depth of the top of the detached slab, we infer that the break-off is recent (5-10 Ma), in good agreement with other geological records.

Effective detachment of an oceanic slab from continental lithosphere is often followed by the upwelling of the asthenosphere through slab gaps, subduction, slab retreat, and eventually volcanism and exhumation of ultra-high-pressure rocks, which are not currently observed in central Iran. On the other hand, the lack of deep seismicity, especially deep extensional events in the Zagros, indicates that the subducted slab does not exert gravitational pull on the base of the continental plate. To reconcile these apparently contradictory observations, we propose that slab break-off in NW Zagros is very young.

Acknowledgments

This research was funded by several IASBS internal grants. M.V. benefited from support provided by the Ministry of Science, Research and Technology of Iran and Laboratoire Géosciences Environnement Toulouse – GET. We acknowledge ISC and INSN for use of their permanent station data. The Zagros01 and Zagros03 arrays were installed by LGIT, Grenoble and IIEES, Tehran. The CIGSIP array was supported by the Strategic Priority Research Program (B) (Grant no. XDB03010802) and the International Partnership Program (GIH21776) of the Chinese Academy of Sciences. The IASBS-CAM arrays were jointly operated by IASBS and

Univ. of Cambridge. Maps were prepared using the Generic Mapping Tools (Wessel & Smith 1998). We thank associate editor Ling Chen, Zhouchuan Huang, and two other anonymous reviewers for their valuable comments and critique of the manuscript.

References

Agard, P., Omrani, J., Jolivet, L., Whitechurch, H., Vrielynck, B., Spakman, W., Monié, P., Meyer, B. and Wortel, R., 2011. Zagros orogeny: a subduction-dominated process. *Geological Magazine*, *148*(5-6), pp. 692-725. https://doi.org/10.1017/S001675681100046X.

Aki, K., Christoffersson, A. and Husebye, E.S., 1977. Determination of the three-dimensional seismic structure of the lithosphere. *Journal of Geophysical Research*, *82*(2), pp. 277-296. https://doi.org/10.1029/JB082i002p00277.

Al-Damegh, K., Sandvol, E., Al-Lazki, A. and Barazangi, M., 2004. Regional seismic wave propagation (Lg and Sn) and Pn attenuation in the Arabian Plate and surrounding regions. *Geophysical Journal International*, *157*(2), pp. 775-795. https://doi.org/10.1111/j.1365-246X.2004.02246.x.

Alinaghi, A., Koulakov, I. and Thybo, H., 2007. Seismic tomographic imaging of P-and S-waves velocity perturbations in the upper mantle beneath Iran. *Geophysical Journal International*, *169*(3), pp. 1089-1102. https://doi.org/10.1111/j.1365-246X.2007.03317.x.

Al-Lazki, A.I., Sandvol, E., Seber, D., Barazangi, M., Turkelli, N. and Mohamad, R., 2004. Pn tomographic imaging of mantle lid velocity and anisotropy at the junction of the Arabian,

Eurasian and African plates. *Geophysical Journal International*, *158*(3), pp. 1024-1040. https://doi.org/10.1111/j.1365-246X.2004.02355.x.

Arvin, S., Sobouti, F., Priestley, K., Ghods, A., Motaghi, K., Tilmann, F. and Eken, T., 2021. Seismic anisotropy and mantle deformation in NW Iran inferred from splitting measurements of SK (K) S and direct S phases. *Geophysical Journal International*, *226*(2), pp.1417-1431. https://doi.org/10.1093/gji/ggab181.

Asudeh, I., 1982. Pn velocities beneath Iran. *Earth and Planetary Science Letters*, *61*(1), pp. 136-142. https://doi.org/10.1016/0012-821X(82)90046-2.

Ballato, P., Mulch, A., Landgraf, A., Strecker, M.R., Dalconi, M.C., Friedrich, A. and Tabatabaei, S.H., 2010. Middle to late Miocene Middle Eastern climate from stable oxygen and carbon isotope data, southern Alborz Mountains, N Iran. *Earth and Planetary Science Letters*, *300*(1-2), pp. 125-138. https://doi.org/10.1016/j.epsl.2010.09.043.

Bijwaard, H., Spakman, W. and Engdahl, E.R., 1998. Closing the gap between regional and global travel time tomography. *Journal of Geophysical Research: Solid Earth*, *103*(B12), pp. 30055-30078. https://doi.org/10.1029/98JB02467.

Chang, S.J., Van Der Lee, S., Flanagan, M.P., Bedle, H., Marone, F., Matzel, E.M., Pasyanos, M.E., Rodgers, A.J., Romanowicz, B. and Schmid, C., 2010. Joint inversion for three-dimensional S velocity mantle structure along the Tethyan margin. *Journal of Geophysical Research: Solid Earth*, *115*(B8). https://doi.org/10.1029/2009JB007204.

Chen, M., Niu, F., Tromp, J., Lenardic, A., Lee, C., Cao, W. and Ribeiro, J., (2017). Lithospheric foundering and underthrusting imaged beneath Tibet. *Nature Communication*, 8, 15659 (2017). https://doi.org/10.1038/ncomms15659.

Chevrot, S., 2002. Optimal measurement of relative and absolute delay times by simulated annealing. *Geophysical Journal International*, *151*(1), pp. 164-171. https://doi.org/10.1046/j.1365-246X.2002.01755.x.

Chiu, H.Y., Chung, S.L., Zarrinkoub, M.H., Mohammadi, S.S., Khatib, M.M. and Iizuka, Y., 2013. Zircon U–Pb age constraints from Iran on the magmatic evolution related to Neo-Tethyan subduction and Zagros orogeny. *Lithos*, *162*, pp. 70-87. https://doi.org/10.1016/j.lithos.2013.01.006.

Davidson, J. P., Hassanzadeh, J., Berzins, R., Stockli, D.F., Bashukooh, B., Turrin, B., and Pandamouz, A., 2004. The geology of Damavand volcano, Alborz Mountains, northern Iran. *Geological Society of America Bulletin*, 116, 16-29. https://doi.org/10.1130/B25344.

Dercourt, J. Ricou, L. E., and Vrielynck, B., 1993. *Atlas Tethys, paleoenvironmental maps*. Elsevier, New York.

Duretz, T., Schmalholz, S.M. and Gerya, T.V., 2012. Dynamics of slab detachment. *Geochemistry, Geophysics, Geosystems*, *13*(3). https://doi.org/10.1029/2011GC004024.

Duretz, T., Gerya, T.V. and May, D.A., 2011. Numerical modelling of spontaneous slab breakoff and subsequent topographic response. *Tectonophysics*, *502*(1-2), pp. 244-256. https://doi.org/10.1016/j.tecto.2010.05.024.

Egan, S.S., Mosar, J., Brunet, M.F. and Kangarli, T., 2009. Subsidence and uplift mechanisms within the South Caspian Basin: insights from the onshore and offshore Azerbaijan region. *Geological Society, London, Special Publications*, *312*(1), pp. 219-240. https://doi.org/10.1144/SP312.11.

Evans, J., Achauer, U., Iyer, H. and Hirahara, K., 1993. Teleseismic velocity tomography using the ACH method: theory and application to continental scale. In: Iver, H.M., and Hirahara, K., (Eds.), *Seismic Tomography: Theory and Practice*, Chapman & Hall., London, pp. 319-360.

François, T., Burov, E., Agard, P. and Meyer, B., 2014. Buildup of a dynamically supported orogenic plateau: Numerical modeling of the Zagros/Central Iran case study. *Geochemistry, Geophysics, Geosystems*, *15*(6), pp. 2632-2654. https://doi.org/10.1002/2013GC005223.

Goes, S., Govers, R. and Vacher, A.P., 2000. Shallow mantle temperatures under Europe from P and S wave tomography. *Journal of Geophysical Research: Solid Earth*, *105*(B5), pp. 11153-11169. https://doi.org/10.1029/1999JB900300.

Guest, B., Horton, B.K., Axen, G.J., Hassanzadeh, J. and McIntosh, W.C., 2007. Middle to late Cenozoic basin evolution in the western Alborz Mountains: Implications for the onset of collisional deformation in northern Iran. *Tectonics*, *26*(6). https://doi.org/10.1029/2006TC002091.

Guest, B., Axen, G.J., Lam, P.S. and Hassanzadeh, J., 2006. Late Cenozoic shortening in the west-central Alborz Mountains, northern Iran by combined conjugate strike-slip and thin-skinned deformation. *Geosphere*, *2*(1), pp. 35-52. https://doi.org/10.1130/GES00019.1.

Hafkenscheid, E., Wortel, M.J.R. and Spakman, W., 2006. Subduction history of the Tethyan region derived from seismic tomography and tectonic reconstructions. *Journal of Geophysical Research: Solid Earth*, *111*(B8). https://doi.org/10.1029/2005JB003791.

Hatzfeld, D. and Molnar, P., 2010. Comparisons of the kinematics and deep structures of the Zagros and Himalaya and of the Iranian and Tibetan plateaus and geodynamic implications. *Reviews of Geophysics*, *48*(2). https://doi.org/10.1029/2009RG000304.

Huang, Z., Wang, L., Xu, M., Zhao, D., Mi, N., and Yu, D., 2019. P and S wave tomography beneath the SE Tibetan Plateau: Evidence for lithospheric delamination. *Journal of Geophysical Research: Solid Earth.* https://doi.org/10.1029/2019JB017430.

Kaviani, A., Mahmoodabadi, M., Rümpker, G., Pilia, S., Tatar, M., Nilfouroushan, F., Yamini-Fard, F., Moradi, A. and Ali, M.Y., 2021. Mantle-flow diversion beneath the Iranian plateau induced by Zagros' lithospheric keel. *Scientific reports*, *11*(1), pp.1-12.

Kaviani, A., Paul, A., Moradi, A., Mai, P.M., Pilia, S., Boschi, L., Rümpker, G., Lu, Y., Tang, Z. and Sandvol, E., 2020. Crustal and uppermost mantle shear wave velocity structure beneath the Middle East from surface wave tomography. *Geophysical Journal International*, 221(2), pp. 1349-1365. https://doi.org/10.1093/gji/ggaa075.

Kaviani, A., Sandvol, E., Moradi, A., Rümpker, G., Tang, Z., and Mai, P. M., 2018. Mantle transition zone thickness beneath the Middle East: Evidence for segmented Tethyan slabs, delaminated lithosphere, and lower mantle upwelling. Journal of Geophysical Research: Solid Earth, 123, 4886–4905. https://doi.org/10.1029/2018JB015627.

Kaviani, A., Paul, A., Bourova, E., Hatzfeld, D., Pedersen, H. and Mokhtari, M., 2007. A strong seismic velocity contrast in the shallow mantle across the Zagros collision zone (Iran). *Geophysical Journal International*, *171*(1), pp. 399-410. https://doi.org/10.1111/j.1365-246X.2007.03535.x.

Karasözen, E., Nissen, E., Bergman, E.A. and Ghods, A., 2019. Seismotectonics of the Zagros (Iran) from orogen-wide, calibrated earthquake relocations. Journal of Geophysical Research: Solid Earth, 124(8), pp.9109-9129. https://doi.org/10.1029/2019JB017336.

Koulakov, I., 2011. High-frequency P and S velocity anomalies in the upper mantle beneath Asia from inversion of worldwide traveltime data. *Journal of Geophysical Research: Solid Earth*, *116*(B4). https://doi.org/10.1029/2010JB007938.

Liotard, J. M., J. M. Dautria, D. Bosch, M. Condomines, M. Mehdizadeh, and J.-F. Ritz, 2008. Origin of the absarokite–banakite association of the Damavand volcano (Iran): Trace elements and Sr, Nd, Pb isotope constraints, *Int. J. Earth Sci.*, 97, 89–102. https://doi.org/10.1007/s00531-006-0159-6.

Maggi, A. and Priestley, K., 2005. Surface waveform tomography of the Turkish–Iranian plateau. *Geophysical Journal International*, *160*(3), pp.1068-1080. https://doi.org/10.1111/j.1365-246X.2005.02505.x.

Mahmoodabadi, M., Yaminifard, F., Tatar, M. and Kaviani, A., 2020. Shear wave velocity structure of the upper-mantle beneath the northern Zagros collision zone revealed by nonlinear teleseismic tomography and Bayesian Monte-Carlo joint inversion of surface wave dispersion and teleseismic P-wave coda. *Physics of the Earth and Planetary Interiors*. https://doi.org/10.1016/j.pepi.2020.106444.

Mahmoodabadi, M., Yaminifard, F., Tatar, M., Kaviani, A. and Motaghi, K., 2019. Upper-mantle velocity structure beneath the Zagros collision zone, Central Iran and Alborz from nonlinear teleseismic tomography. *Geophysical Journal International*, *218*(1), pp. 414-428. https://doi.org/10.1093/gji/ggz160.

Maupin, V., 2020. Combining asynchronous data sets in regional body-wave tomography. *Geophysical Journal International*, *224*(1), pp. 401-415. https://doi.org/10.1093/gji/ggaa473.

McQuarrie, N. and van Hinsbergen, D.J., 2013. Retro-deforming the Arabia-Eurasia collision zone: Age of collision versus magnitude of continental subduction. *Geology*, *41*(3), pp. 315-318. https://doi.org/10.1130/G33591.1.

Mohammadi, N., Sodoudi, F., Mohammadi, E., and Sadidkhouy, A., 2013. New constraints on lithospheric thickness of the Iranian plateau using converted waves. Journal of Seismology, 17:883–895. https://doi.org/10.1007/s10950-013-9359-2.

Motaghi, K., Shabanian, E. and Kalvandi, F., 2017a. Underplating along the northern portion of the Zagros suture zone, Iran. *Geophysical Journal International*, *210*(1), pp.375-389. https://doi.org/10.1093/gji/ggx168.

Motaghi, K., Shabanian, E., Tatar, M., Cuffaro, M. and Doglioni, C., 2017b. The south Zagros suture zone in teleseismic images. *Tectonophysics*, *694*, pp. 292-301. https://doi.org/10.1016/j.tecto.2016.11.012.

Motaghi, K., Tatar, M., Shomali, Z.H., Kaviani, A. and Priestley, K., 2012. High resolution image of uppermost mantle beneath NE Iran continental collision zone. *Physics of the Earth and Planetary Interiors*, *208*, pp. 38-49. https://doi.org/10.1016/j.pepi.2012.07.006.

Omrani, J., Agard, P., Whitechurch, H., Benoit, M., Prouteau, G. and Jolivet, L., 2008. Arc-magmatism and subduction history beneath the Zagros Mountains, Iran: a new report of adakites and geodynamic consequences. *Lithos*, *106*(3-4), pp. 380-398. https://doi.org/10.1016/j.lithos.2008.09.008.

Paige, C.C. and Saunders, M.A., 1982. LSQR: An algorithm for sparse linear equations and sparse least squares. *ACM Transactions on Mathematical Software (TOMS)*, *8*(1), pp. 43-71. https://doi.org/10.1145/355984.355989.

Paul, A., Hatzfeld, D., Kaviani, A., Tatar, M. and Péquegnat, C., 2010. Seismic imaging of the lithospheric structure of the Zagros mountain belt (Iran). *Geological Society, London, Special Publications*, *330*(1), pp. 5-18. https://doi.org/10.1144/SP330.2.

Paul, A., Kaviani, A., Hatzfeld, D., Vergne, J. and Mokhtari, M., 2006. Seismological evidence for crustal-scale thrusting in the Zagros mountain belt (Iran). *Geophysical Journal International*, *166*(1), pp. 227-237. https://doi.org/10.1111/j.1365-246X.2006.02920.x.

Pirouz, M., Avouac, J.P., Hassanzadeh, J., Kirschvink, J.L. and Bahroudi, A., 2017. Early Neogene foreland of the Zagros, implications for the initial closure of the Neo-Tethys and kinematics of crustal shortening. *Earth and Planetary Science Letters*, *477*, pp. 168-182. https://doi.org/10.1016/j.epsl.2017.07.046.

Priestley, K., McKenzie, D., Barron, J., Tatar, M. and Debayle, E., 2012. The Zagros core: deformation of the continental lithospheric mantle. *Geochemistry, Geophysics, Geosystems*, *13*(11). https://doi.org/10.1029/2012GC004435.

Radjaee, A., Rham, D., Mokhtari, M., Tatar, M., Priestley, K. and Hatzfeld, D., 2010. Variation of Moho depth in the central part of the Alborz Mountains, northern Iran. *Geophysical Journal International*, *181*(1), pp. 173-184. https://doi.org/10.1111/j.1365-246X.2010.04518.x.

Rahmani, M., Motaghi, K., Ghods, A., Sobouti, F., Talebian, M., Ai, Y. and Chen, L., 2019. Deep velocity image of the north Zagros collision zone (Iran) from regional and teleseismic tomography. *Geophysical Journal International*, *219*(3), pp. 1729-1740. https://doi.org/10.1093/gji/ggz393.

Rastgoo, M., Rahimi, H., Motaghi, K., Shabanian, E., Romanelli, F. and Panza, G.F., 2018. Deep structure of the Alborz Mountains by joint inversion of P receiver functions and dispersion curves. *Physics of the Earth and Planetary Interiors*, 277, pp. 70-80. https://doi.org/10.1016/j.pepi.2018.01.011.

Ren, Y. and Shen, Y., 2008. Finite frequency tomography in southeastern Tibet: evidence for the causal relationship between mantle lithosphere delamination and the north–south trending rifts. *Journal of Geophysical Research: Solid Earth*, *113*(B10). https://doi.org/10.1029/2008JB005615.

Sadeghi-Bagherabadi, A., Margheriti, L., Aoudia, A. and Sobouti, F., 2018. Seismic anisotropy and its geodynamic implications in Iran, the easternmost part of the Tethyan Belt. *Tectonics*, *37*(12), pp.4377-4395.https://doi.org/10.1029/2018TC005209.

Şengör, A.M.C., and Natal'in, B.A., 1996. Paleotectonics of Asia: fragments of a synthesis. *The tectonic evolution of Asia*, pp. 486-640.

Shabanian, E., Acocella, V., Gioncada, A., Ghasemi, H. and Bellier, O., 2012. Structural control on volcanism in intraplate post collisional settings: Late Cenozoic to Quaternary examples of Iran and Eastern Turkey. *Tectonics*, 31(3). https://doi.org/10.1029/2011TC003042.

Shad Manaman, N., Shomali, H. and Koyi, H., 2011. New constraints on upper-mantle S-velocity structure and crustal thickness of the Iranian plateau using partitioned waveform inversion. *Geophysical Journal International*, *184*(1), pp. 247-267. https://doi.org/10.1111/j.1365-246X.2010.04822.x.

Shomali, Z.H., Keshvari, F., Hassanzadeh, J. and Mirzaei, N., 2011. Lithospheric structure beneath the Zagros collision zone resolved by non-linear teleseismic tomography. *Geophysical Journal International*, *187*(1), pp. 394-406. https://doi.org/10.1111/j.1365-246X.2011.05150.x.

Stampfli, G.M. and Borel, G.D., 2004. The TRANSMED transects in space and time: constraints on the paleotectonic evolution of the Mediterranean domain. In: Cavazza, W., Roure, F., Spakman, W., Stampfli, G.M., Ziegler, P.A. (Eds.), *The TRANSMED Atlas. The Mediterranean region from crust to mantle*. Springer., Berlin, Heidelberg, pp. 53-80. https://doi.org/10.1007/978-3-642-18919-7_3.

Stampfli, G.M. and Borel, G.D., 2002. A plate tectonic model for the Paleozoic and Mesozoic constrained by dynamic plate boundaries and restored synthetic oceanic isochrons. *Earth and Planetary Science Letters*, *196* (1-2), pp. 17-33. https://doi.org/10.1016/S0012-821X(01)00588-X.

Stöcklin, J., 1968. Structural history and tectonics of Iran: a review. *AAPG bulletin*, *52*(7), pp. 1229-1258. https://doi.org/10.1306/5D25C4A5-16C1-11D7-8645000102C1865D.

Van der Meer, D.G., Van Hinsbergen, D.J. and Spakman, W., 2018. Atlas of the underworld: Slab remnants in the mantle, their sinking history, and a new outlook on lower mantle viscosity. *Tectonophysics*, *723*, pp. 309-448. https://doi.org/10.1016/j.tecto.2017.10.004.

van Hunen, J. and Allen, M.B., 2011. Continental collision and slab break-off: A comparison of 3-D numerical models with observations. *Earth and Planetary Science Letters*, *302*(1-2), pp. 27-37. https://doi.org/10.1016/j.epsl.2010.11.035.

Verdel, C., Wernicke, B.P., Hassanzadeh, J. and Guest, B., 2011. A Paleogene extensional arc flare up in Iran. *Tectonics*, *30*(3). https://doi.org/10.1029/2010TC002809.

Wessel, P. and Smith, W.H., 1998. New, improved version of Generic Mapping Tools released. *Eos, Transactions American Geophysical Union*, *79*(47), pp. 579-579. https://doi.org/10.1029/98EO00426.

Table1: Summary of network and data information used in this study

Network name	No of stations	Operation period	Sensors type	Operating agency
Zagros01	64	Nov 2000 to Apr 2001	STRECKEISEN STS2, CHINESE CDJ, LENNARTZ LE3D	IIEES,Tehran LGIT, Grenoble
Zagros03	35	May -Nov 200 3	GURALP CMG40, LENNARTZ LE3D	IIEES,Tehran LGIT, Grenoble

CIGSIP	63	Sep 2013 - Oct 2014	TRILIUM and GURALP broadband	IGGCAS, Beijing GSI,Tehran IASBS, Zanjan
IASBS-CAM1	23	Aug 2008 - Jul 2012	CMG-3ESP, CMG-3TD Guralp system	IASBS, Zanjan Cambridge, UK
IASBS-CAM2	17	Sep 2014 Jun 2016	CMG-3ESP, CMG-3TD Guralp system	IASBS, Zanjan Cambridge, UK
IRSC permanent stations	85	2012 - 2018 with one year gaps	Mostly broadband sensors	IRSC, Tehran
INSN permanent stations	17	2012-2014 2018-2019	Various Guralp broadbands	INSN, Tehran

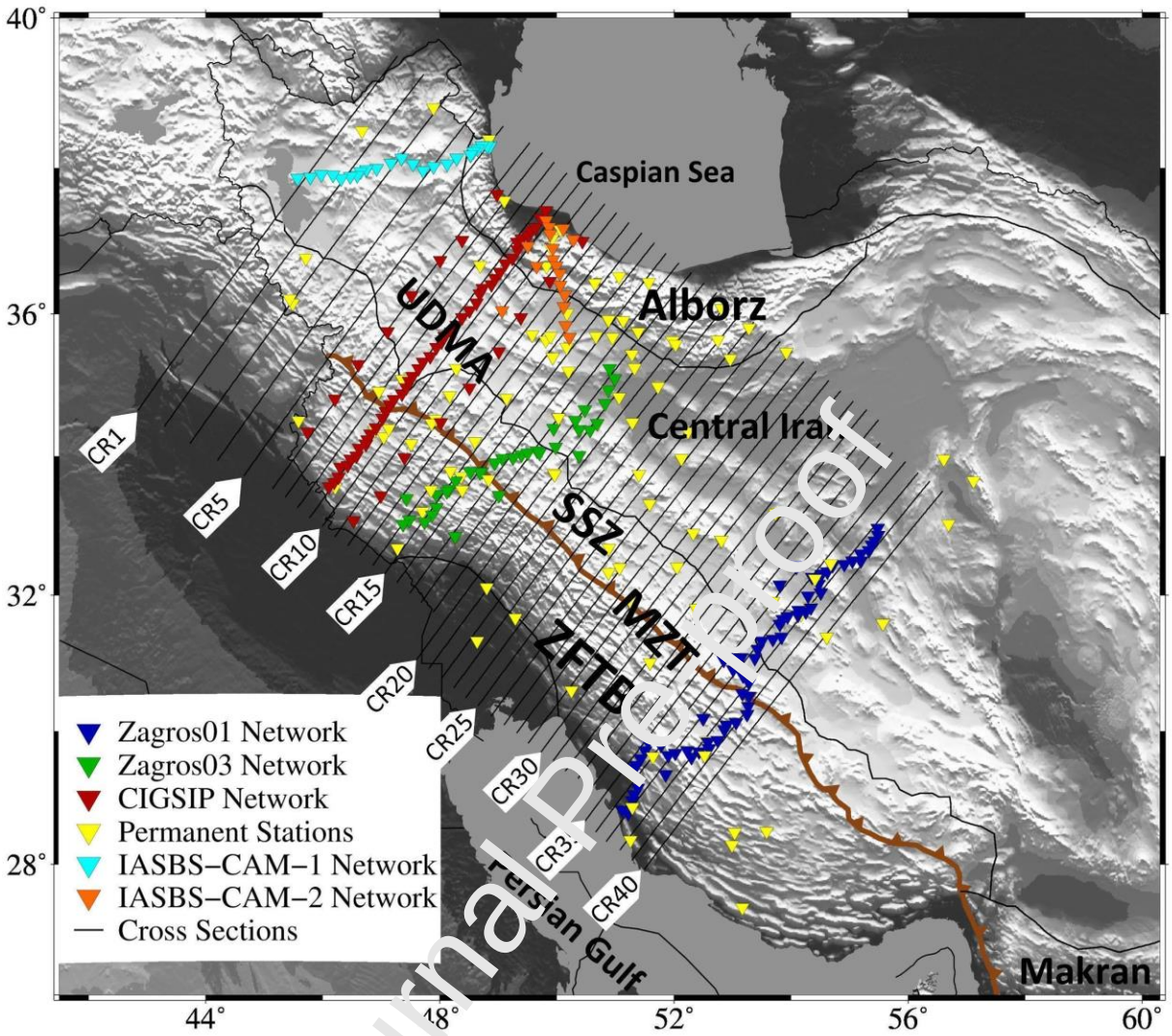

Figure 1. Map showing the seismic networks used in this study as well as the major tectonic units: Zagros Fold and Thrust Belt (ZFTB), Main Zagros Thrust (MZT), Alborz Mountains, Sanandaj-Sirjan Zone (SSZ), Urmia-Dokhtar Magmatic Arc (UDMA), the Central Iran Microblock, and Makran Subduction Zone. The positions of the cross-sections, numbered from 1 to 40, are also shown with black solid lines.

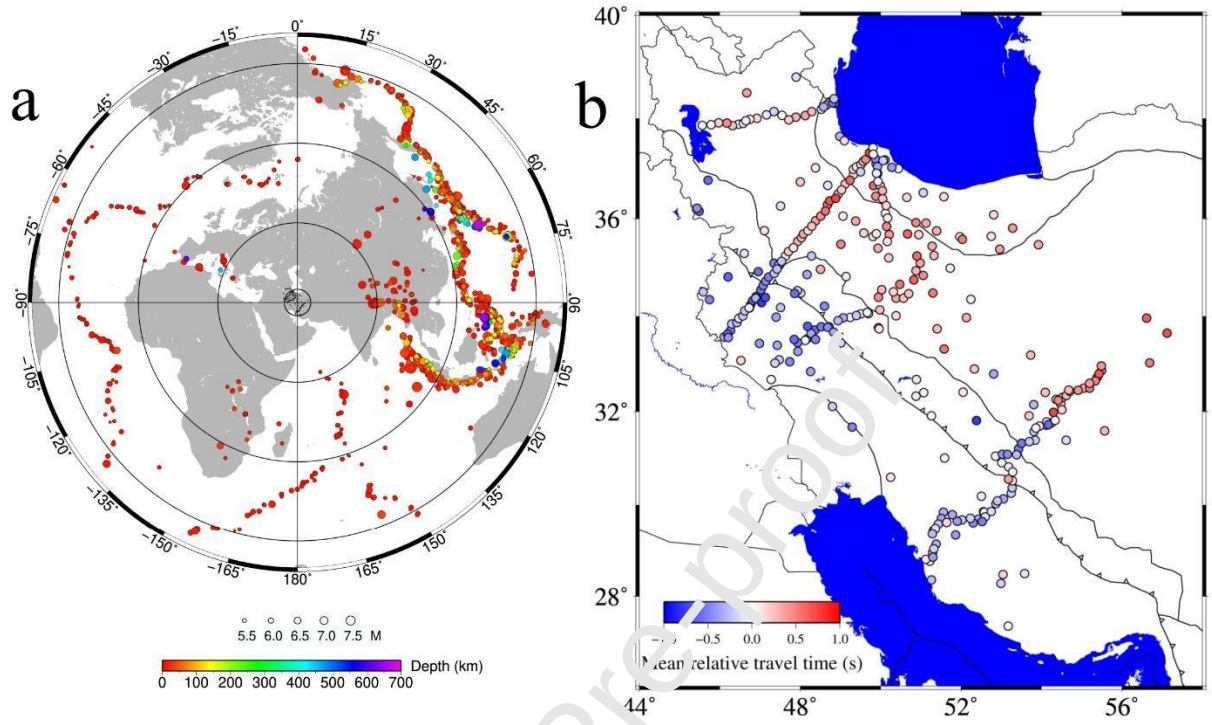

Figure 2. (a) Map showing the epicenters of teleseismic events used in this study. Epicentral distances are computed from the center of our tomographic grid. (b) Map showing average station travel time residuals.

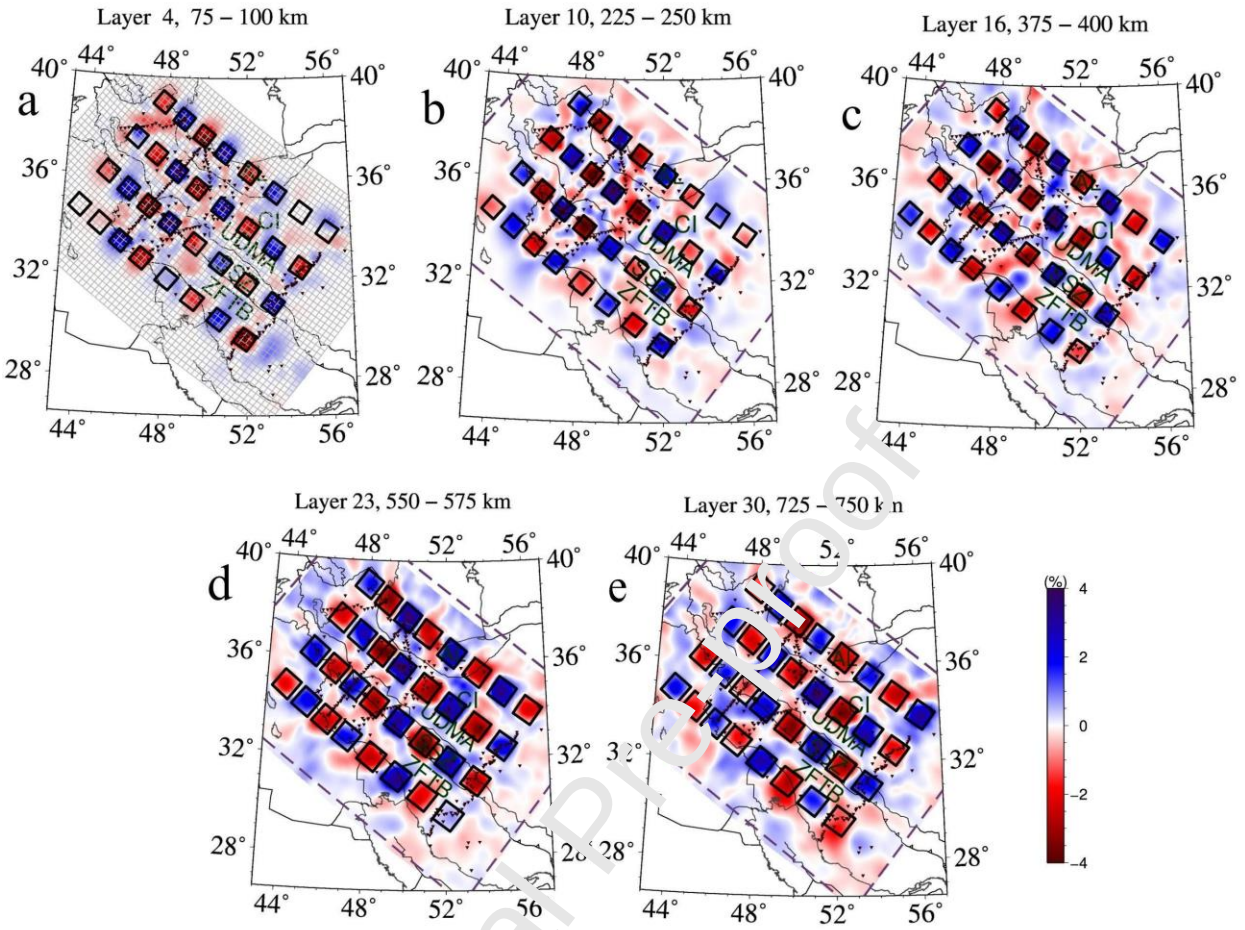

Figure 3. The results of the synthetic five-layer spike inversion test at different depths. The horizontal grid shows the model discretization. Solid squares represent the synthetic model, with alternating positive and negative anomalies.

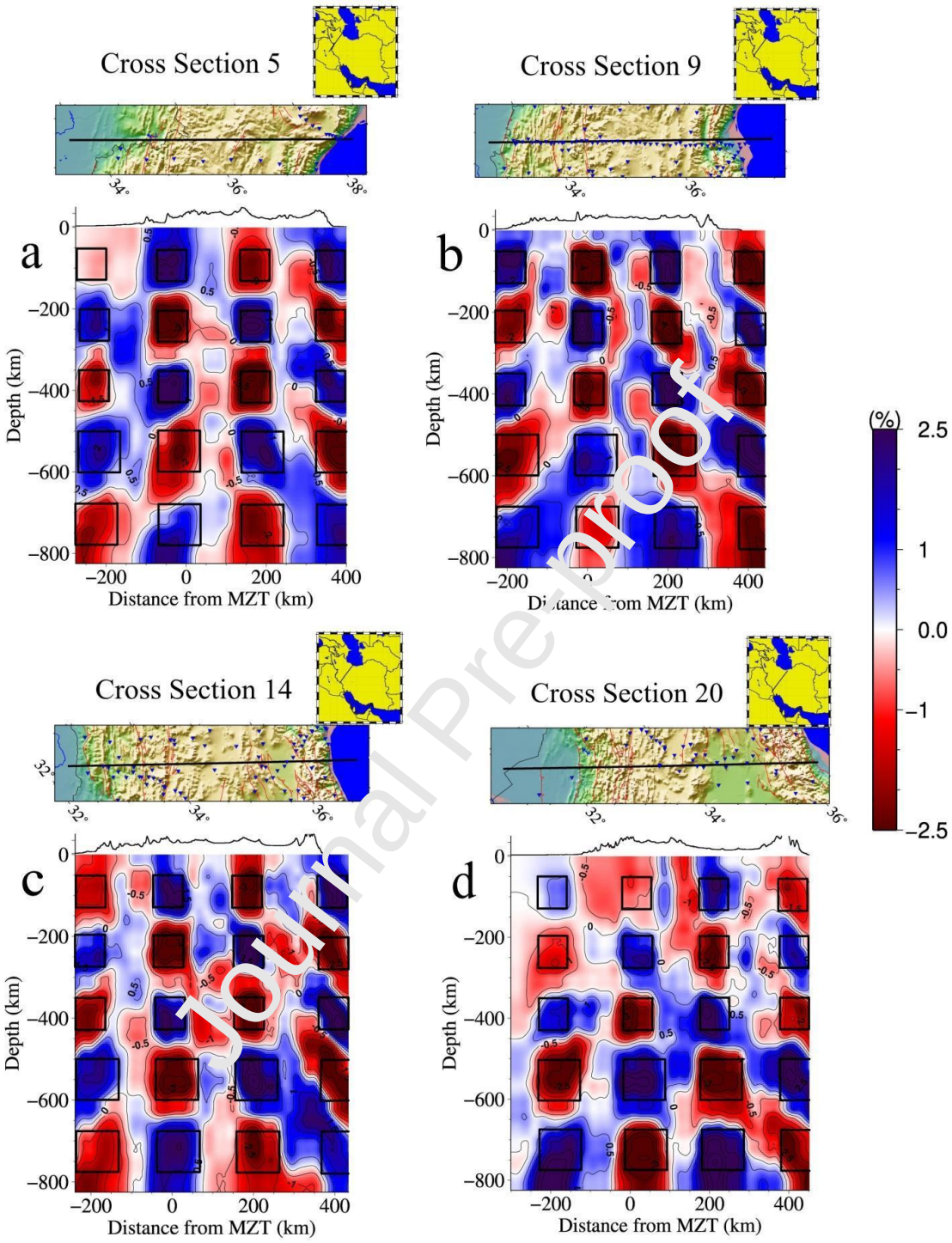

Figure 4. Results of the spike test inversion along 7 cross-sections. Location and surface topography are displayed on the top of each cross-section. Solid squares represent the anomalies in the synthetic model.

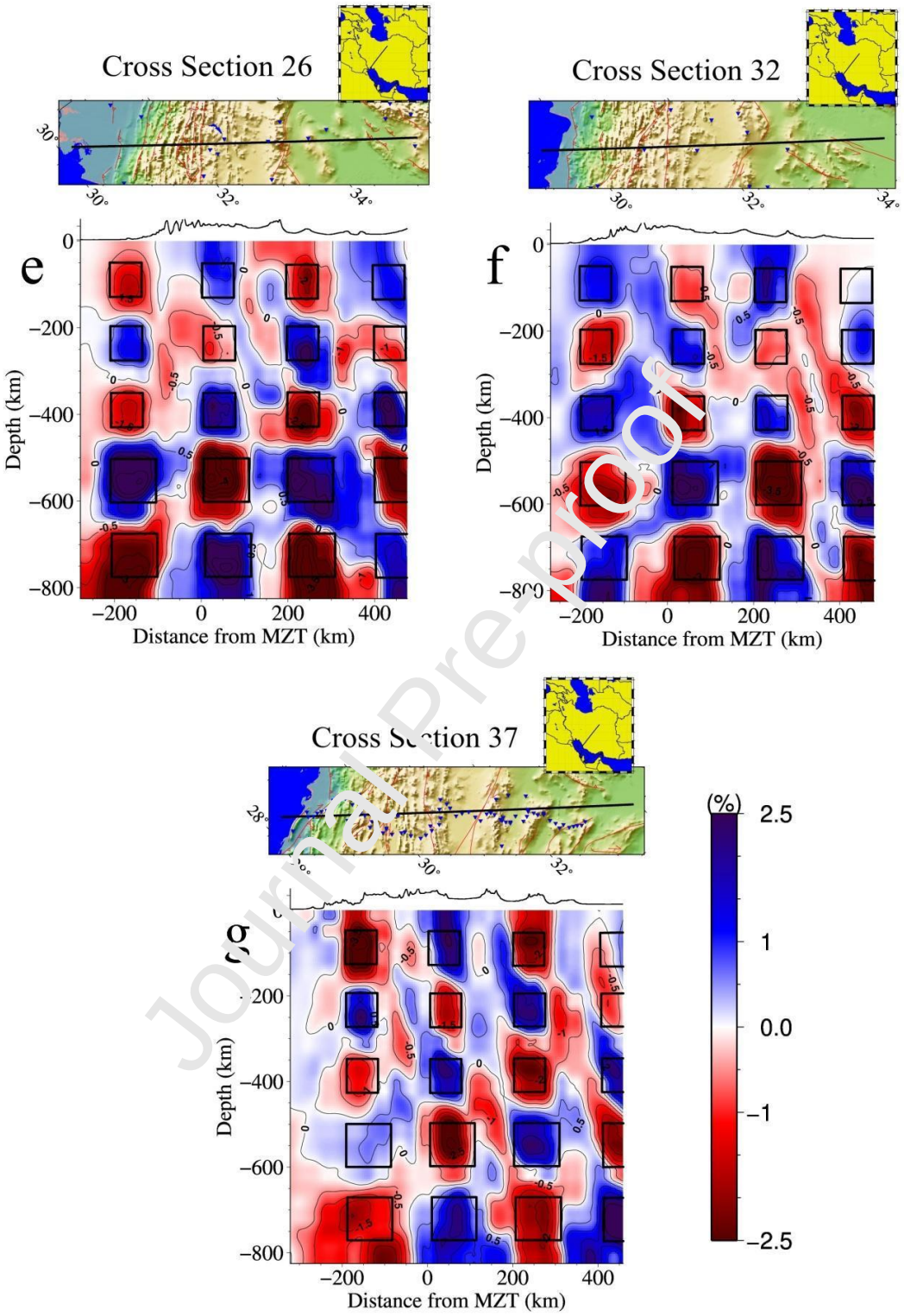

Figure 4. Continued.

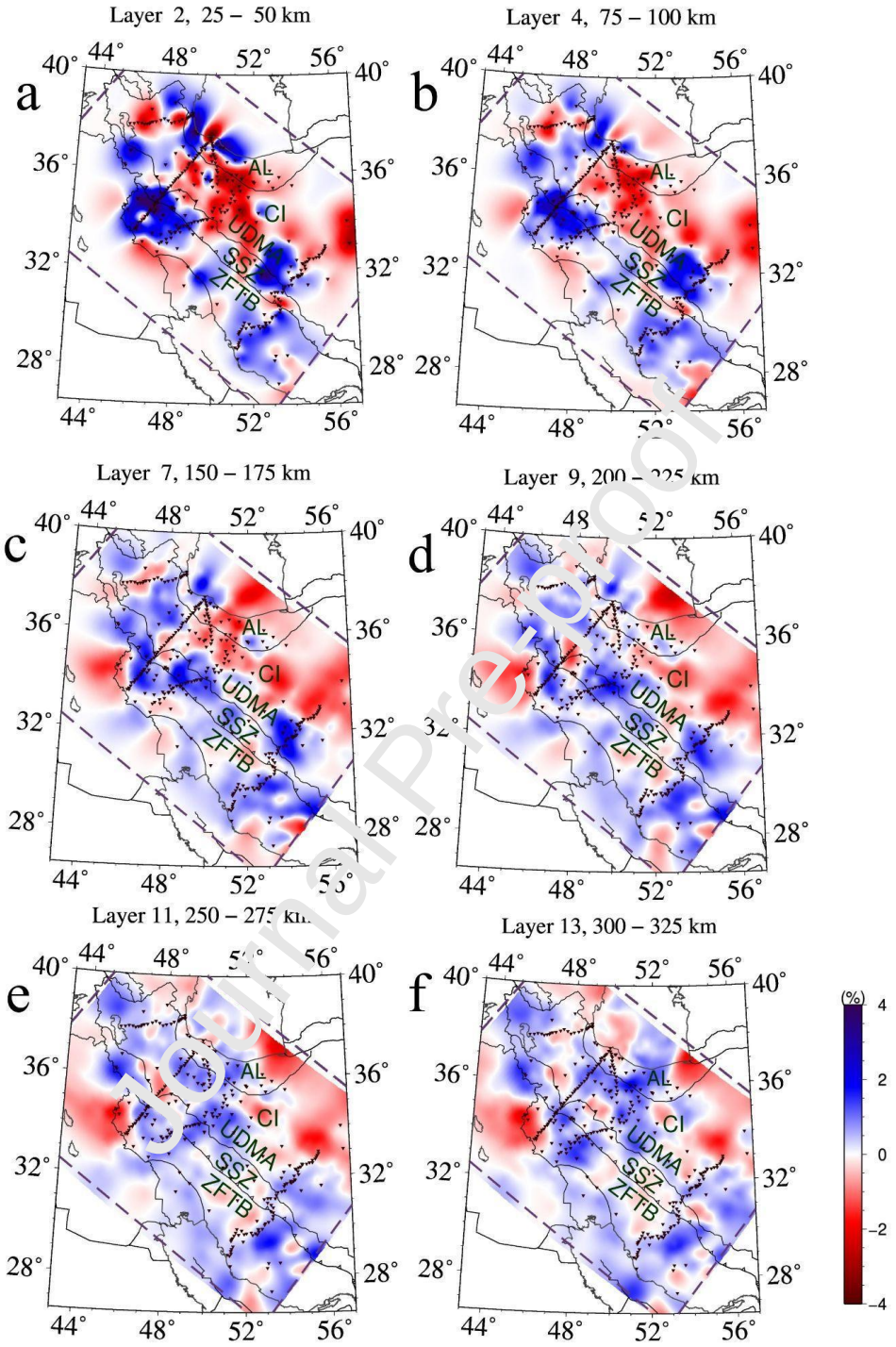

Figure 5. Horizontal sections at 12 different depths in the final model.

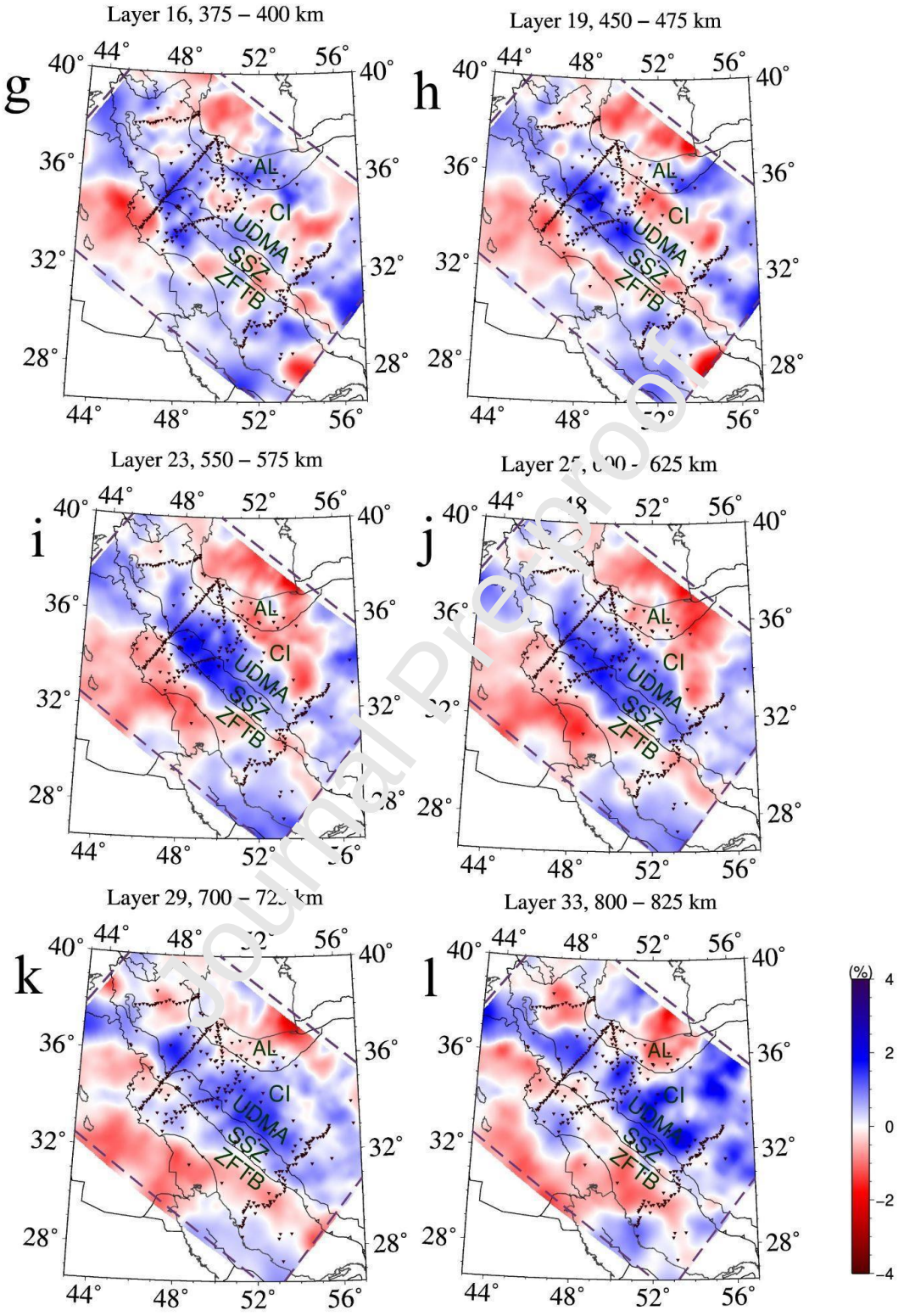

Figure 5. Continued.

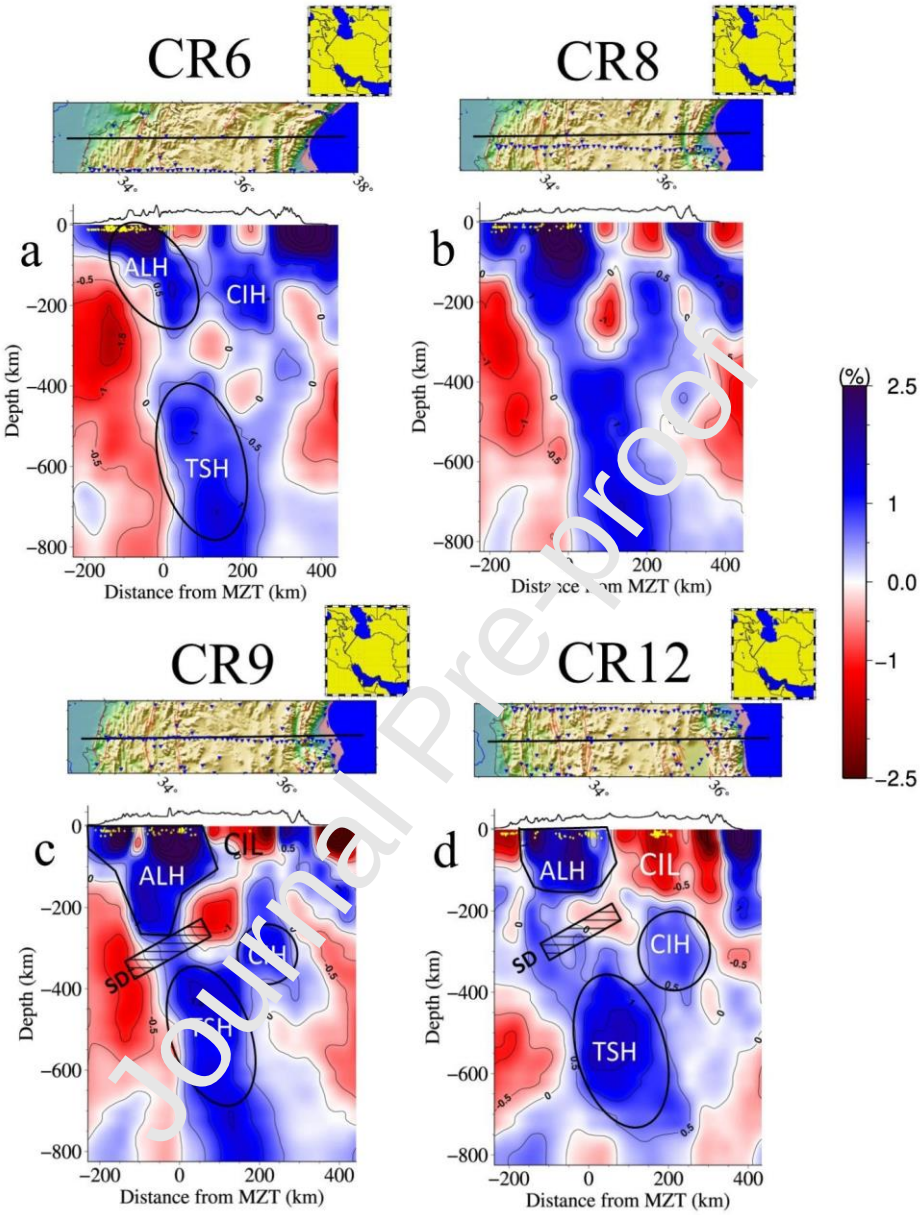

Figure 6. Four vertical cross sections through the western part of the tomographic model. Figure details are the same as in Fig. 4. The major velocity anomalies discussed in the text are outlined: ALH (Arabian lithosphere High), CIL (central Iran Low), CIH (Central Iran High) and TSH (Tethyan Slab High). The hatched rectangle SD denotes the detachment of the subducted slab. Yellow dots represent the hypocenter of earthquakes after Karasözen et al. (2019).

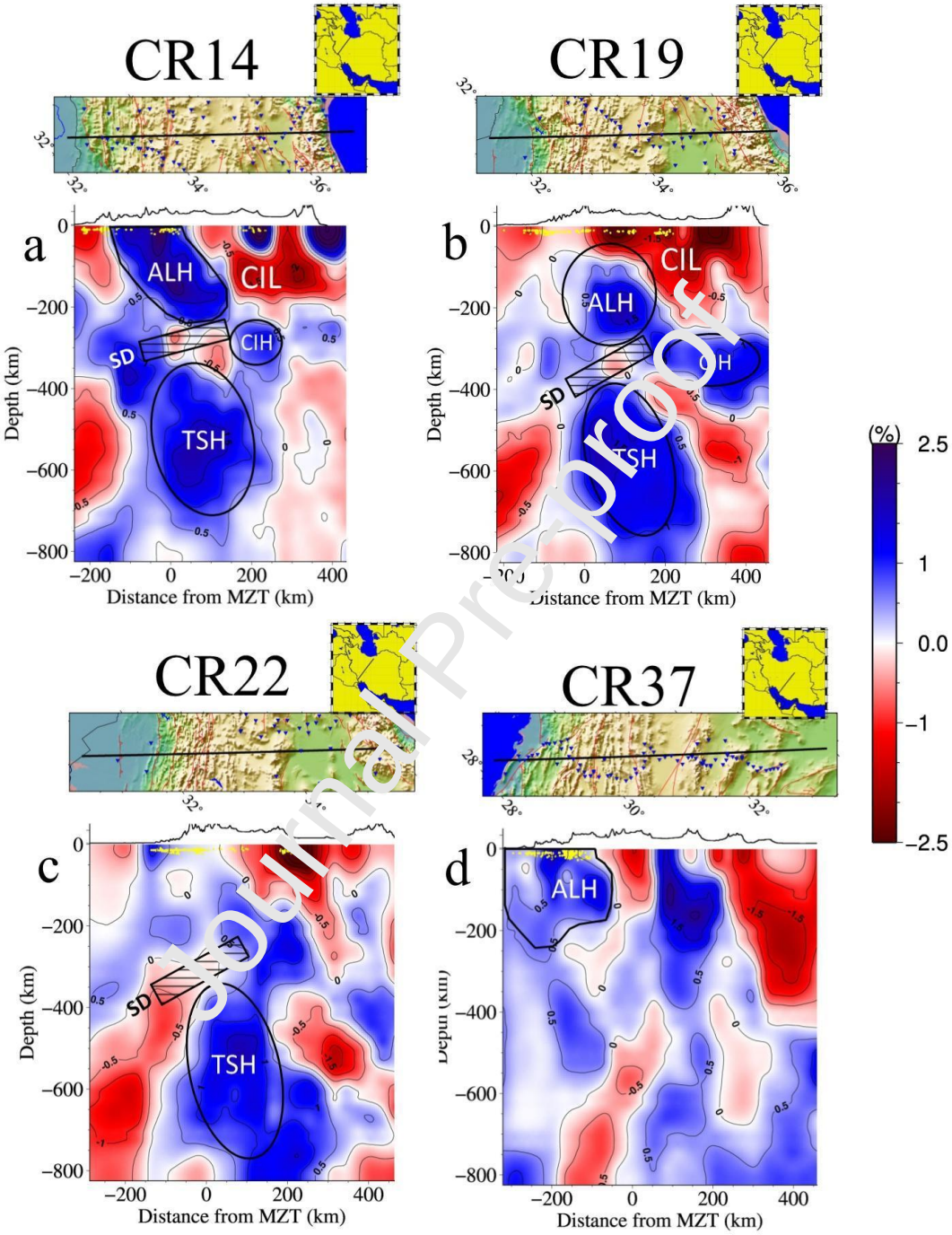

Figure 7. Four vertical cross sections through the eastern part of the tomography model. Figure details are the same as in Fig. 6. SD denotes the slab detachment, which is more clearly seen in central Zagros.

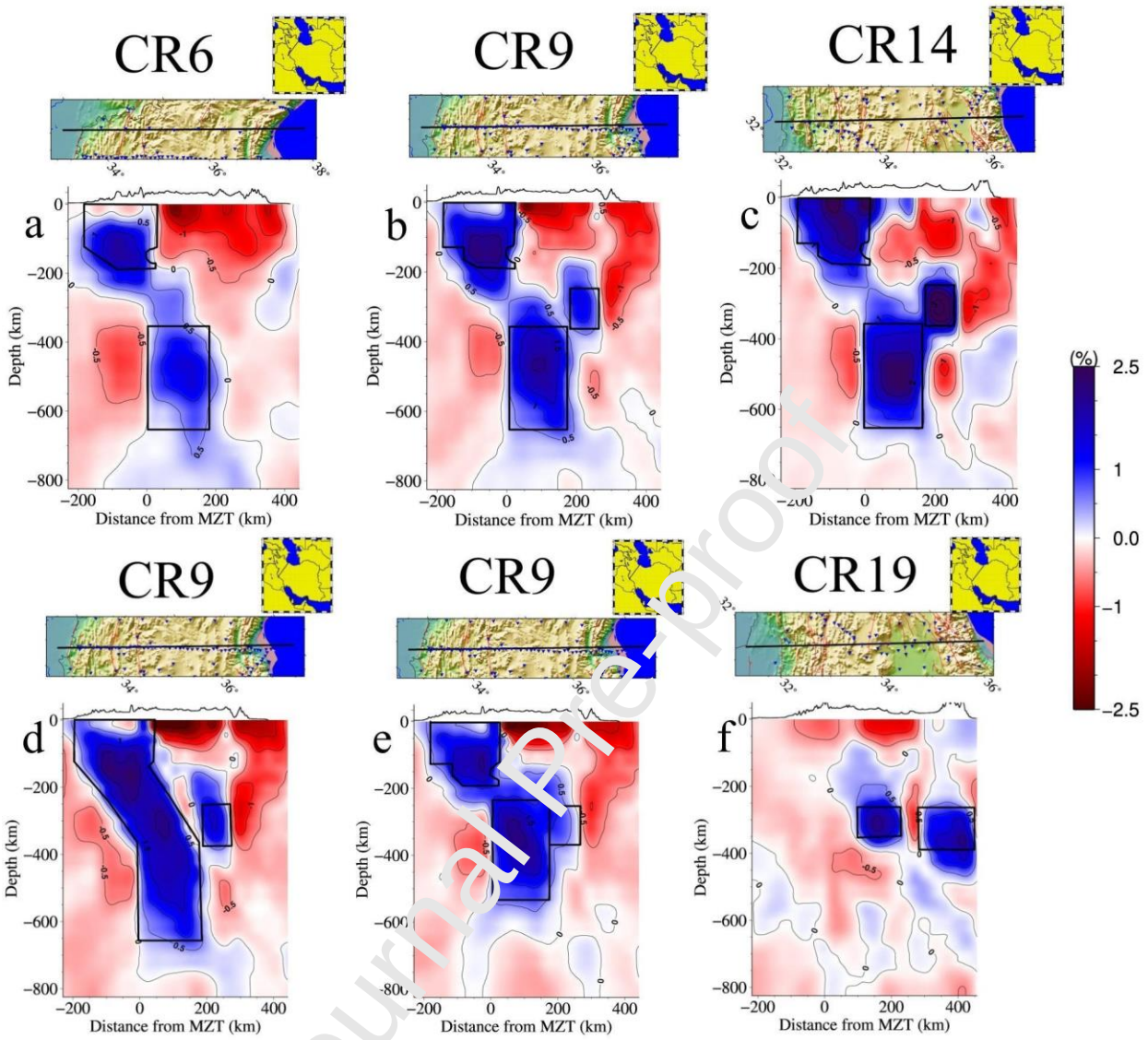

Figure 8. Simplified synthetic tests to infer the robustness of the anomalies in NW Zagros. Cross sections a, b, and c represent a model with 150-km separation between AHL and TSH. Cross section d shows the synthetic model for a continuous slab. Cross section e illustrates a synthetic model with a 25-km separation between modelled ALH and TSH bodies and cross section f shows two small high-velocity synthetic bodies with a horizontal separation of 100 km, showing the resolving power of tomography where the CIH anomalies reside.

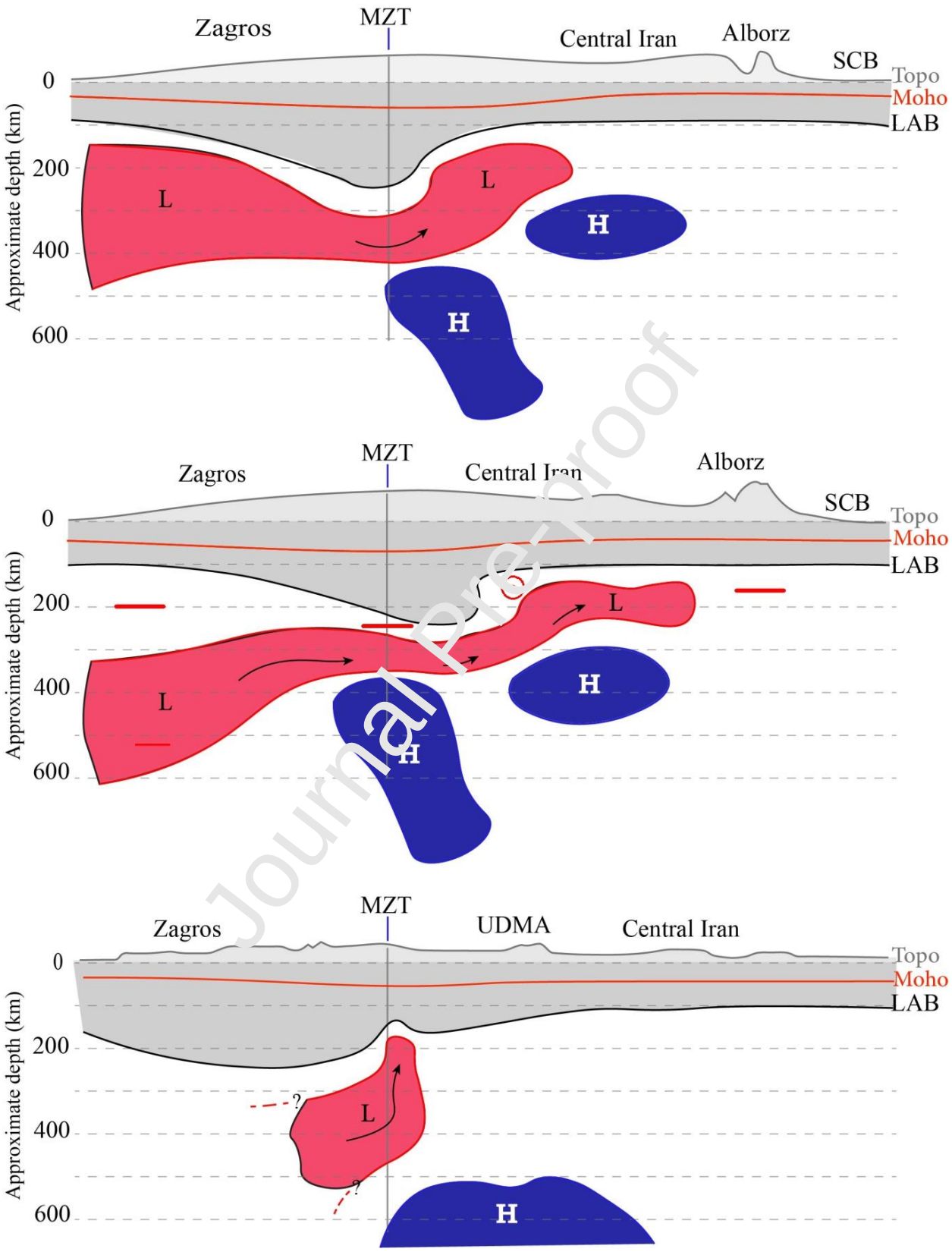

Figure 9. Three schematic cross-sections of the upper mantle beneath the collision zone that illustrate our interpretation of the tomography results. Profiles from top to bottom roughly correspond to the locations of the CIGSIP, Zagros03, and Zagros01 arrays, respectively. The splitting fast axes (red bars and circle-and-dot) shown in the middle profile represent the overall pattern of anisotropy as derived from the recent investigations referenced in the text. The arrows show the possible direction of the mantle flow field taking into account our tomographic interpretations, as well as inferences from seismic anisotropy.

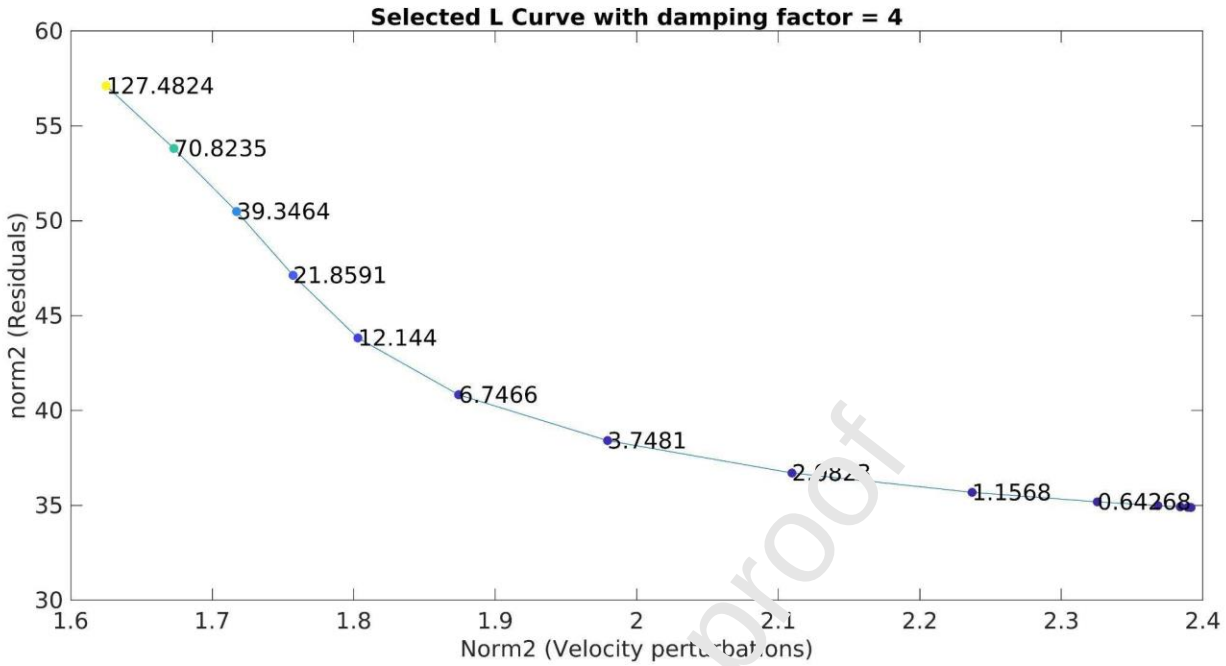

Figure S1. A selected L-Curve for evaluating the damping and smoothing factors. This curve was calculated for damping factor =4, The values of the smoothing factor are shown on the curve. Based on this diagram, we chose a best smoothing factor of 12.144.

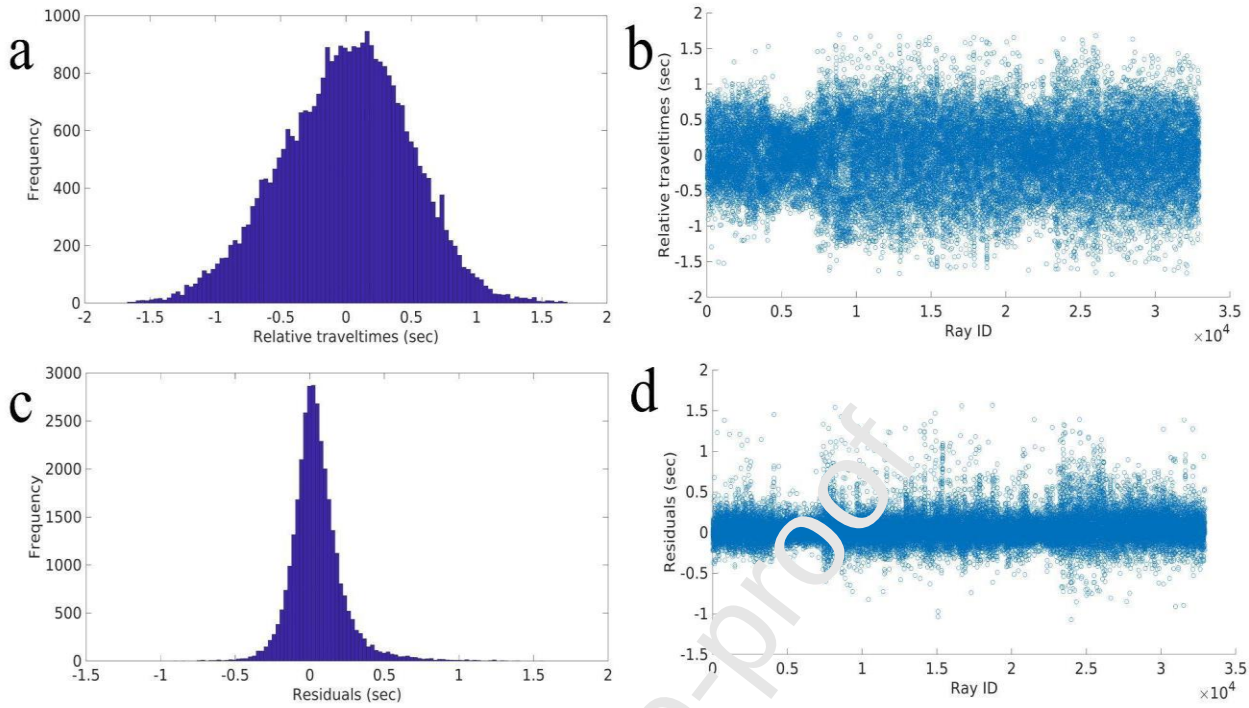

Figure S2. Histogram and scatter plot of relative travel times before (a and b) and after (c and d) inversion.

Mohammad Veisi: Conceptualization, Methodology, Software, Formal analysis, Data Curation, Writing, Validation. **Farhad Sobouti:** Supervision, Conceptualization, Methodology, Resources, Writing, Funding acquisition. **Sébastien Chevrot**: Conceptualization, Methodology, Software, Resources, Writing, Funding acquisition. **Madjid Abbasi:** Methodology, Supervision**. Esmaeil Shabanian**: Conceptualization, Writing.

Declaration of interests

☒ The authors declare that they have no known competing financial interests or personal relationships
that could have appeared to influence the work reported in this paper.

☐The authors declare the following financial interests/personal relationships which may be considered
as potential competing interests:

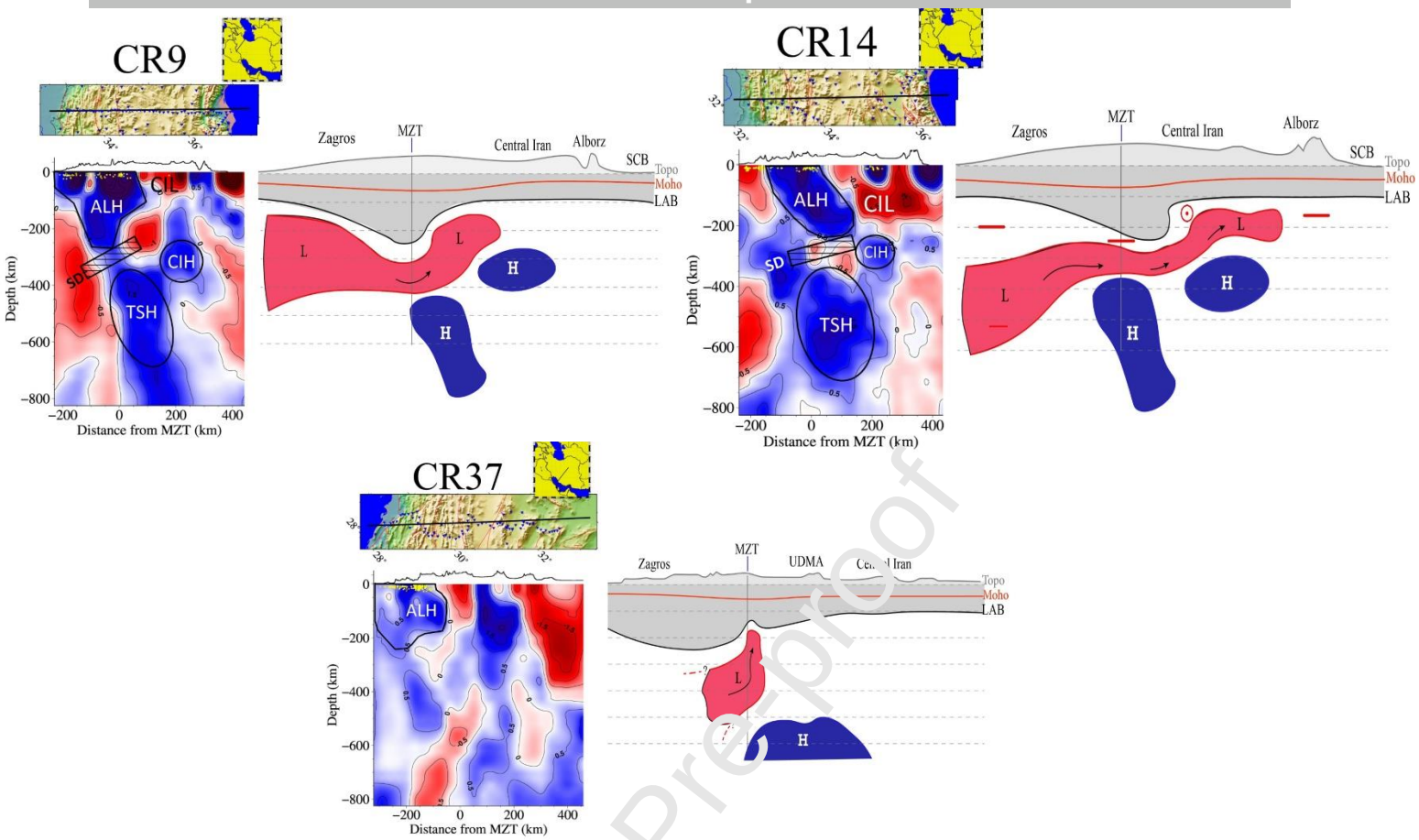

Three vertical cross sections and their schematic cross-sections representing our main finding. The major velocity anomalies are outlined: ALH (Arabian lithosphere High), CIL (central Iran Low), CIH (Central Iran High) and TSH (Tethyan Slab High). The hatched rectangle SD denotes the detachment of the subducted slab, red bars and circle and dot represent the splitting fast axis.

We map the lateral variations of P-wave velocity beneath the Zagros collision zone in Iran down to 800 km depth by regional travel time tomography. Our tomographic study documents variations of lithospheric thickness between the Zagros and central Iran and a post-collisional slab detachment around 250 km depth. If we assume that the detachment occurred right beneath the base of the subducted Arabian continental margin, then the maximum thickness of the continental root must be no greater than 225 km. This would imply a doubling of the Zagros lithosphere as a result of collision. The absence of high-velocity anomalies far north from the MZT at the lithospheric depth range indicates that the lithosphere thickening has not propagated into the interior of central Iran. The high-velocity anomalies at 200-300 km depth beneath central Iran suggest the presence of fragments of delaminated mantle lithosphere. They also suggest post-collisional slab break-off in central Zagros that seems to be at an earlier stage in NW Zagros compared to central Zagros. From the shallow depth of the top of the detached slab, we infer that the break-off is recent (5-10 Ma), in good agreement with geological records. Effective detachment of an oceanic slab from continental lithosphere is often followed by the upwelling of the asthenosphere through slab windows, eduction, slab retreat, and eventually volcanism and exhumation of ultra-high-pressure rocks, which are not currently observed in central Iran. On the other hand, lack of deep seismicity, especially deep extensional events in the Zagros, indicates that the subducted slab does not exert gravitational pull on the base of the continental plate to reconcile these apparently contradictory observations, we propose that slab break-off in NW Zagros is very young.

Highlights

- Upper mantle structure of the Zagros collision zone via teleseismic tomography.
- Evidence for a thicker lithosphere beneath the Zagros versus thinner lithosphere in the surrounding regions.
- Slab detachment near the base of the thickened Zagros lithosphere.
- Seismological evidence for mantle lithospheric delamination beneath central Iran.